Atomic-level modeling of the early stage of copper oxidation

A thesis proposal by

Minyoung Lee

November 13, 2008

205 Scaife Hall

Department of Mechanical Engineering

Carnegie Mellon University

Thesis committee

Dr. Alan McGaughey, Committee Chair and Assistant Professor of Mechanical Engineering

Dr. Judith C. Yang, Associate Professor of Mechanical Engineering and Materials Science, University of Pittsburgh

Dr. John Kitchin, Assistant Professor of Chemical Engineering

Dr. O. Burak Ozdoganlar, Associate Professor of Mechanical Engineering

Contents

1 Introduction

1.1 Motivation

Copper surfaces exposed to oxygen environments and devices with copper-copper oxide interfaces are used in applications to promote efficient catalytic reactions for the synthesis of bio-chemical compounds[1] and methanol for fuel cells,[2] and the gate dielectric of thin film transistors.[3] It is thus important to understand the mechanism on the surface oxidation. It was traditionally believed that the oxide grows as a uniform layer on a clean metal surface.[4] Yang *et al.*,[5] however, as shown in Fig. 1, found by *in situ* transmission electron microscopy (TEM) that oxide islands nucleate and grow on the Cu(100) surface. Based on their observations, the general sequence of oxidation is molecular oxygen dissociation and adsorption (chemisorption), surface reconstruction, oxide island nucleation, island growth, and finally thin film growth.[6] The oxide grows into substrate metal as well as grows vertically and horizontally.[6,7]

The shape of the oxide islands depends on the copper surface structure, temperature, and oxygen partial pressure. Zhou *et al.*[8,9] observed various nano-structures of copper (II) oxide (Cu_2O) islands on the Cu(100) surface, as shown in Fig. 2. At a temperature of 600°C [see Fig. 2(c)], they observed an elongated shape the nano-rod structure, whose size and

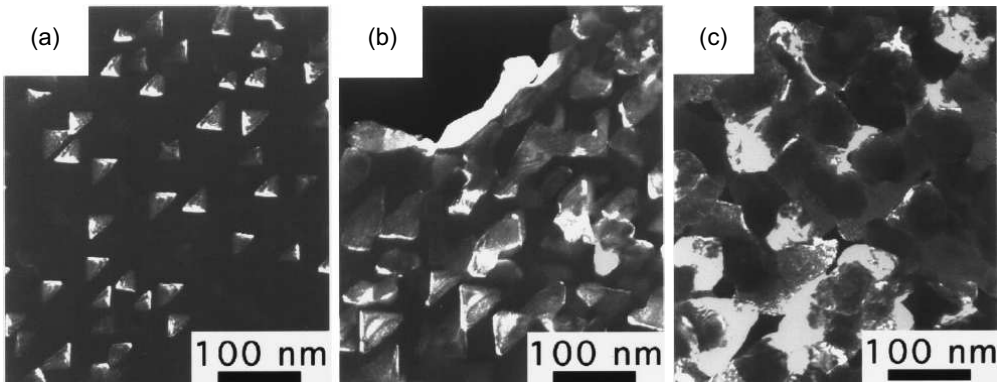

Figure 1: *In situ* TEM images for copper (II) oxide (Cu_2O) nucleation and growth on the Cu(100) surface at 350°C and 0.1 Torr;[5] (a) Cu_2O island nucleation, (b) Cu_2O island growth. (c) Coalescence of Cu_2O islands.

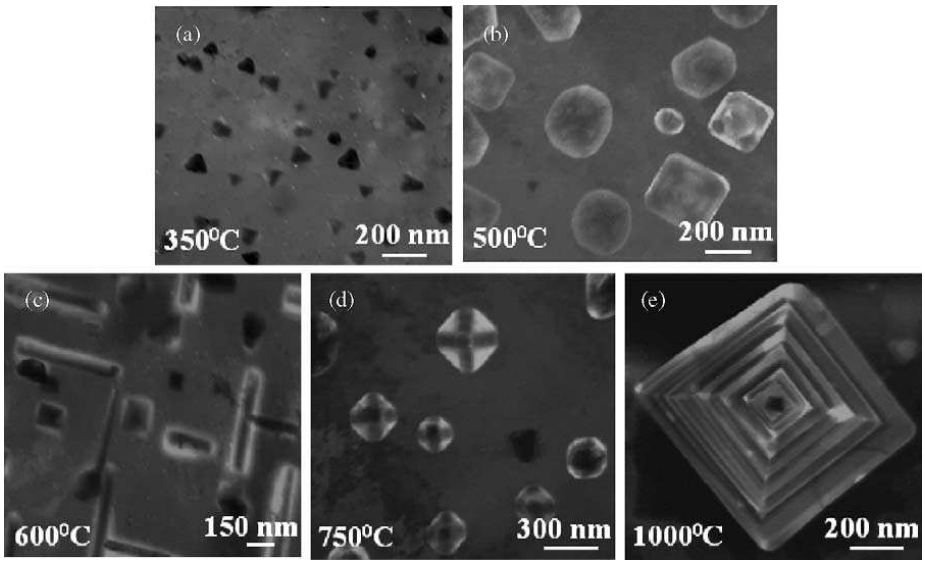

Figure 2: Ultra high vacuum tunneling electron microscopy (UHV-TEM) images of Cu_2O island formed on the Cu(100) surface at different temperatures.[9] (a) Triangular shape at 350°C. (b) Square shape at 500°C. (c) Nano-rod shape at 600°C. (d) Pyramid shape at 700°C. (e) Pyramid with flat terrace at 1000°C.

aspect ratio are determined by the oxidation time.[8] At the higher temperatures, the oxide islands have pyramid shapes, as shown in Figs. 2(d) and 2(e). The growth of the nano-rod structure (and other morphologies) is an example of self-assembly, a process in which a structure is built from the bottom-up without direct intervention.[10] To take advantage of the different morphologies, we need to better understand the atomic-level mechanisms of copper oxidation.

The initial oxygen adsorption on a copper surface has been investigated by experiment[5–8,11–26] and *ab initio* (*i.e.*, first principles) calculation.[27–48] Initially, cluster model calculations were dominant.[27,29,31] However, with increasing computer power, surface models with periodic boundary conditions (k-point sampling) are now widely used.[38,39,42–48] The low index Cu surfaces [(100), (110), and (111)] are frequently chosen.[27,32,33,37] Alatalo *et al.* investigated the oxygen adsorption energy[38] and the dynamics of oxygen molecule disso-

ciation and atomic oxygen adsorption[44] by *ab initio* molecular dynamics simulation on the Cu(100) surface. Kangas *et al.* calculated adsorption energies on the missing-row reconstructed Cu(100) surface for various combinations of on- and sub-surface oxygen adsorption and found that sub-surface oxygen adsorption makes the entire system more energetically stable under high oxygen coverage.[42] Other than this limited work, there is little understanding of how the reconstructed surface transitions to an oxide phase.

There have been many experimental and theoretical studies to find the driving force behind the Cu(100) reconstruction. In the missing-row reconstruction $[(2\sqrt{2}\times\sqrt{2})R45^{\circ}]$, every fourth row of surface copper atoms is squeezed out.[12,14] Experimental techniques including lower energy electron diffraction (LEED),[11] scanning tunneling microscopy (STM),[12,14] surface extended xray absorption fine structure (SEXAFS),[13] angle-resolved ultraviolet photoemission spectroscopy (ARUPS),[16] and photoelectron diffraction (PhD)[18] have been applied. The nucleation and growth of the oxide islands does not begin until after the surface reconstruction is complete. It has been found that the stable surface structure varies with temperature by x-ray scattering measurement and density functional theory (DFT) calculation.[26] Below 473K, the missing-row reconstructed Cu(100) surface is stable but the $c(2\times2)$ structure with 0.25 ML disordered Cu vacancies is observed for temperatures between 473K and 1000K.[26] The mechanisms linking the surface reconstruction to copper-oxide formation (cuprite) are unknown.[48] Their identifying is a first step towards predicting how and why the oxide island shape varies with temperature.

1.2 Objectives

The goal of my proposed research is to determine how the missing-row reconstructed Cu(100) surface transitions to oxide island formation. I will apply DFT calculations to

1. Investigate the energetics of atomic and molecular oxygen adsorption on the missing-row reconstructed Cu(100) surface,

2. Determine the structure of further oxygen-induced reconstruction of the missing-row reconstructed Cu(100) and unreconstructed Cu(110) surfaces,

3. investigate the nature of oxygen embedment into the missing-row reconstructed Cu(100) surface to determine how the reconstructed surface transitions to an oxide phase, and

4. Assist in the development of a Cu/Cu_2O charge transfer interatomic potential, which will allow for the modeling of much larger systems than those accessible by DFT calculation.

In Section 2, validation work is presented for the DFT-predicted surface structure based on experimental measurement of the unreconstructed and reconstructed Cu(100) surfaces. In Section 3, the completed and proposed work on adsorption energetics is presented. In Section 4 discusses the investigations of the oxygen-induced reconstruction under different condition. Section 5 discusses the oxygen embedment into the Cu(100) surface and the plan for further investigation on the (110) and (111) surfaces. In Section 6, the current results and plan for the molecular dynamic simulations are presented. The outcomes and schedule of the proposed work are presented in Section 7.

1.3 Collaboration

My work is a part of a DOE-funded collaborative research project between researchers at CMU, the University of Pittsburgh, and the University of Florida. The objective is to develop a kinetic Monte Carlo (KMC) code for modeling oxidation phenomena on metal surfaces using multiple levels of theory and experimental measurements that can be directly compared to experimental results. The KMC code will be parameterized by the DFT calculations and molecular dynamic simulation. The work scope and cooperation are shown in Fig. 3. In addition to the objectives listed above, my work will be used to produce input parameters for the KMC code.

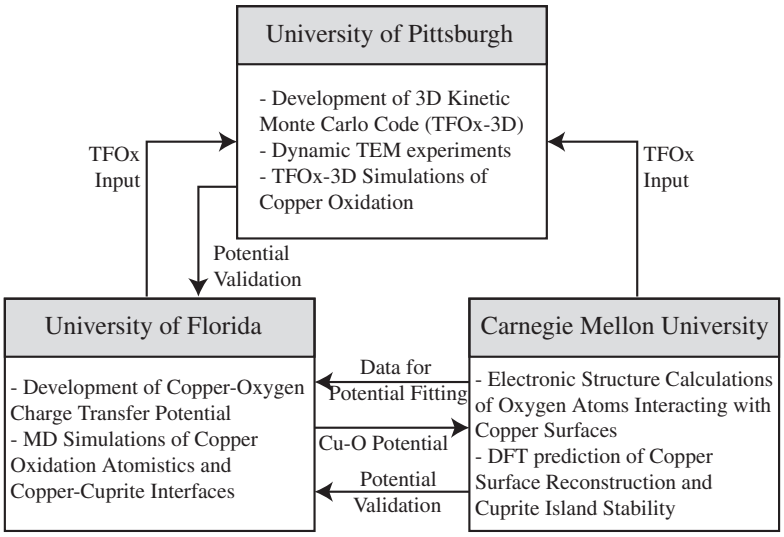

Figure 3: Collaboration flow chart.

2 Validation of DFT calculation on Cu(100) unreconstructed and reconstructed surface structures

2.1 Transformation from the missing-row reconstruction to $c(2\times2)$ with 0.25 ML disordered vacancy

When a copper surface is exposed to an oxygen environment, oxygen molecules will approach the surface, dissociate,[32,33,38] and adsorb on the next-nearest-neighbor hollow sites, as shown in Fig. 4(a).[49] The oxygen coverage is defined as the ratio of the number of oxygen-occupied four-fold hollow sites to the total number of four-fold hollow sites. If one hollow site is occupied by an oxygen atom out of four hollow sites, the oxygen coverage of the surface is 0.25 ML (ML = mono-layer). It was believed that, as the oxygen coverage approaches 0.5 ML, the $c(2\times2)$-O^{-1} phase always evolves into the missing-row reconstruction $[p(2\sqrt{2}\times\sqrt{2})R45°\text{-}2O^{-2}]$.[12,18,50] Iddir *et al.*,[26] however, found that there is another transition structure than the missing row reconstruction on the Cu(100) surface. They used the *in situ*

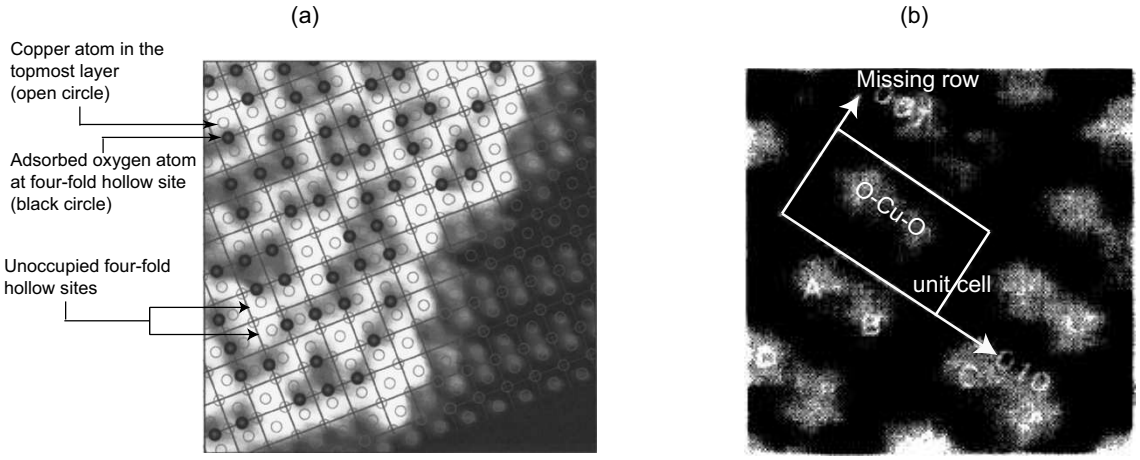

Figure 4: Scanning tunneling microscope (STM) images; (a) $c(2\times2)$-O^{-1}.[49] The area of this STM image is 55×55 Å^2. The black circles are adsorbed oxygen atoms at four-fold hollow site and open circles are copper atoms on the topmost layer of the Cu(100) surface. (b) $p(2\sqrt{2}\times\sqrt{2})R45°\text{-}2O^{-2}$.[12] The area of this STM image is 15×15 Å^2. The unit cell is shown as a white square and the missing row direction is (001) direction. The bright region inside the unit cell indicates a oxygen-copper-oxygen chain.

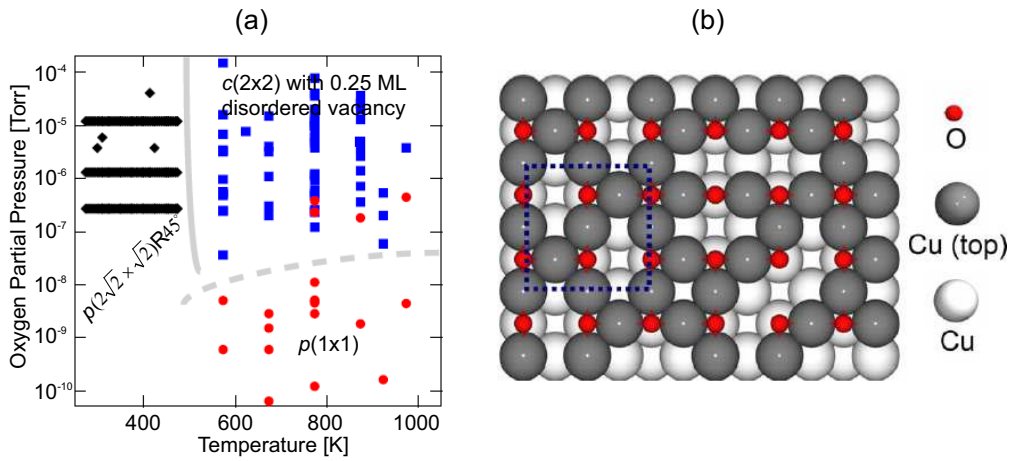

Figure 5: (a) Surface phase diagram for Cu(100)-oxygen at different temperature and pressure conditions[26] The solid line is an equilibrium phase boundary between the $p(2\sqrt{2} \times \sqrt{2})R45°$-$2O^{-2}$ and $c(2\times2)$ with 0.25 ML disordered vacancy phases. The dashed line is the hysteretic boundary for oxygen adsorption and desorption. The oxygen coverage is 1.0 ML for $p(1\times1)$ and 0.5 ML for both $p(2\sqrt{2} \times \sqrt{2})R45°$-$2O^{-2}$ and $c(2\times2)$ with 0.25 ML disordered vacancy. (b) $c(2\times2)$ with 0.25 ML disordered vacancy structure[26] The dashed square indicates the unit cell. The small red spheres are oxygen atoms and big spheres are copper atoms. The topmost copper atoms are colored with dark grey.

synchrotron x-ray scattering method to examine oxygen adsorption on the Cu(100) surface for different oxygen partial pressures and temperatures, and constructed the surface phase diagram shown in Fig. 5(a). Note that the missing-row reconstruction is more stable than other surface structures at temperatures below $\sim$ 500 K. However, for temperatures above $\sim$ 500 K and oxygen partial pressures above 10^{-7} Torr, the missing-row reconstruction is transformed to the $c(2\times2)$ with 0.25 ML vacancy disorder. The $c(2\times2)$ with 0.25 ML vacancy disorder structure is made by relocating the copper atom between two oxygen atoms to one of the vacancies in the missing row, as shown in Fig. 5(b). For oxygen partial pressures below 10^{-8} Torr, the $p(1\times1)$ structure is observed more frequently. As the oxygen partial pressure increases above 10^{-8}, oxygen desorption occurs and the $p(1\times1)$ structure transforms into the $c(2\times2)$ with vacancy disorder.

2.2 Introduction to density functional theory

Density functional theory (DFT) is an *ab initio* calculation method based on quantum-mechanical theory that can be used to investigate the electronic structure of a many-particle system. Density functional theory is based on the Hohenberg-Kohn theorem, which shows the existence of a one-to-one mapping between the ground-state electron density and the ground-state wave function of a many-particle system.[51] Density functional theory is typically implemented for condensed-matter phases using the Kohn-Sham method. In this approach, the system properties of an inhomogeneous system of interacting electrons are predicted based on the properties of a homogeneous system of non-interacting electrons.[52]

Many software packages exist for performing DFT calculations.[53–57] In this work, the Vienna Ab-initio Simulation Package (VASP)[53] is used. VASP performs *ab initio* quantum mechanical calculations using plane-wave basis sets,[58,59] which are computationally efficient for metals, metal-oxide interfaces, and semiconductors.

The VASP calculations are performed using ultra-soft pseudo potentials with the generalized gradient approximation (GGA).[60,61] The GGA predicts total energies, atomization energies, energy barriers, and structural energy differences for solids[61] (including copper)

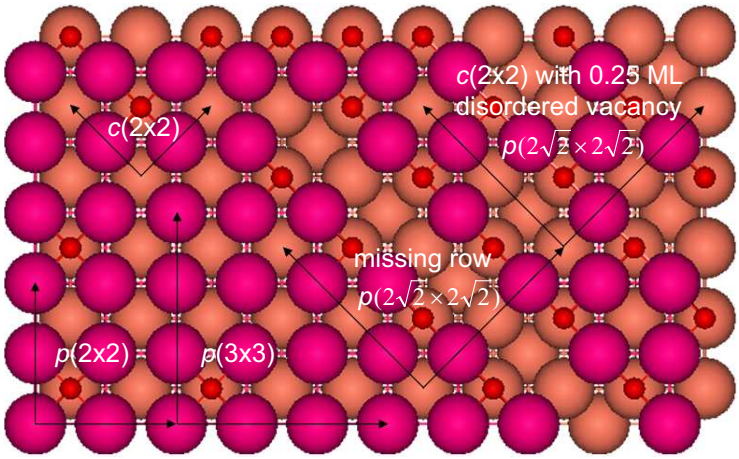

Figure 6: Examples of surface indeces used in the proposed work on Cu(100) surface. The big spheres are copper atoms and small spheres are oxygen atoms. The arrows show the unit cells. The copper atoms on the top layer are colored differently than those on the lower layers.

that are in better agreement with experiments and high-level theory (cluster calculations) than the local density approximation (LDA).[52] Spin-averaged calculations are performed for all single-point energy calculations and structural relaxations. The energy cut-off is 300 eV and the k-point mesh is generated by the Monkhorst-Pack scheme.[62]

In a DFT calculation, a surface structure is modeled using a unit cell that is repeated periodically. The unit cells used in this work are shown in Fig. 6. In the notation $p(3\times3)$, p means that the unit cell is built based on the nearest neighbor distance in the x- and y-directions (lattice constant/$\sqrt{2}$) and 3×3 means that unit cell size is three times the nearest neighbor distance. The extent of the $c(2\times2)$ unit cell is twice the lattice constant in the x- and y- directions.

2.3 DFT prediction and comparison to experiment

In preliminary work, I have investigated the energetics and morphologies of unreconstructed $[c(2\times2)]$ and missing-row reconstruction $[p(2\sqrt{2}\times\sqrt{2})]$ surfaces by DFT calculation. This comparison will show the differences before and after the reconstruction on the Cu(100) surface. Both the unreconstructed and reconstructed surfaces are first relaxed and then the structural parameters shown in Fig. 7 are measured. The simulation cell includes five copper layers and the oxygen coverage is 0.5 ML. The bottom copper layer is fixed and

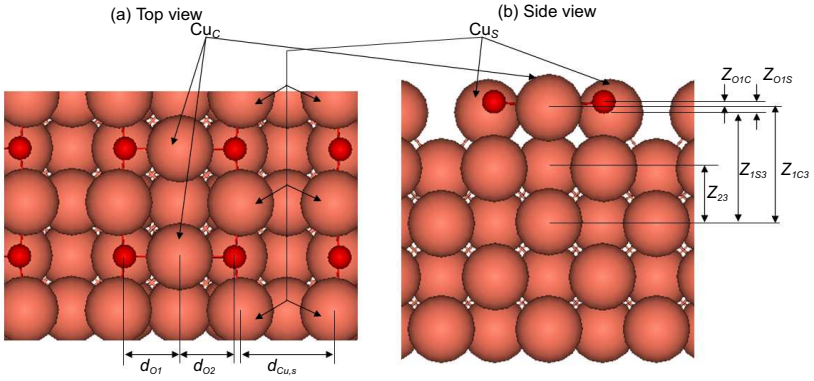

Figure 7: Structural parameters of Cu(100) reconstructed (missing row) surface at 0.5 ML.[18] (a) Distances between copper and oxygen atoms. (b) Vertical distances between oxygen atoms and copper layers.

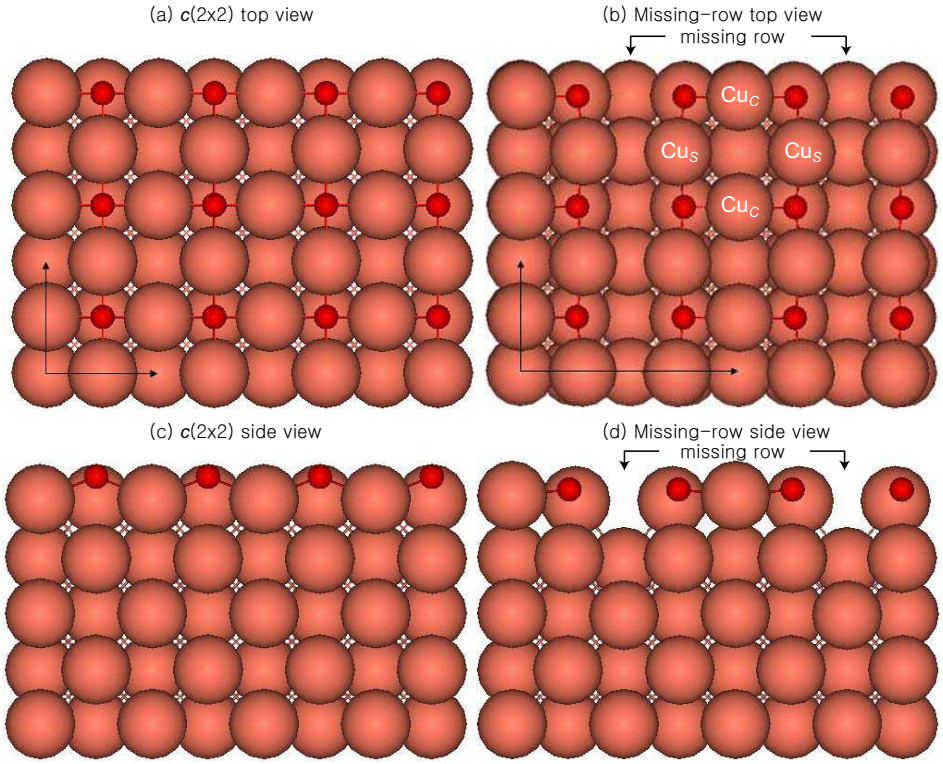

Figure 8: Comparison between unreconstructed and reconstructed structures on the Cu(100) surface. The arrows indicate the unit cell. (a) Relaxed c(2×2) structure top view. (b) Relaxed missing-row reconstruction $[p(2\sqrt{2} \times \sqrt{2})]$ top view. (c) c(2×2) structure cross-section view. (d) Relaxed missing-row reconstruction $[p(2\sqrt{2} \times \sqrt{2})]$ cross-section view.

the other copper layers and the oxygen atoms can move during the structural relaxation.

The relaxed structures are shown in Figs. 8(a)-(d). The surface copper atoms are missing in every fourth row in the missing-row reconstruction. In Figs. 8(b) and 8(d), some of the copper atoms are located at the step-edges next to the missing row. The subscript "S" is used for the structural parameters related to these copper atoms (Cu_S). Likewise, "C" is used to identify the structural parameters related with the topmost copper atoms (Cu_C), which are located between the copper atoms at the step-edges.

The structural parameters measured from the relaxed structures are presented in Table 1. The interatomic distance between the oxygen and copper atoms (d_{O1} and d_{O2}) for the reconstructed surface is slightly bigger than that of unreconstructed surface and the inter-atomic distance between the copper atoms at the step-edge ($d_{Cu,S}$) is smaller than that for the unreconstructed surface. The inter-layer distances (z_{1C3} and z_{23}) indicate that the top-

	$d_{Cu,S}$ [Å]	d_{O1} and d_{O2} [Å]	z_{23} [Å]	z_{1C3} [Å]	z_{O1C} [Å]
Unreconstructed	3.650	1.825	1.804	3.714	0.734
Reconstructed	3.166	1.865	1.811	3.881	0.205

Table 1: Comparison of relaxed structural parameter values between the unreconstructed and reconstructed (missing-row reconstruction) Cu(100) surfaces at an oxygen coverage of 0.5 ML calculated by DFT.

	d_O [Å]	z_{23} [Å]	z_{1S3} [Å]	z_{1C3} [Å]	z_{O1S} [Å]	z_{O1C} [Å]
DFT	0.04	1.81	3.72	3.88	0.37	0.21
PhD[18]	0.04 +0.04/-0.08	1.83 +0.30/-0.20	3.71 +0.30/-0.20	3.97 ±0.30	0.17 ±0.10	0.09 +0.16/-0.19
LEED[11]	0.00	1.84	3.88	3.78	0.10	0.20

Table 2: Comparison between the structural parameter values for the reconstructed (missing-row reconstruction) Cu(100) surface at an oxygen coverage 0.5 ML from DFT calculations and experimental results (PhD: photoelectron diffraction, LEED: low energy electron diffraction).

most copper layer of the missing-row reconstruction moves 0.167 Å upward and that the upward movement does not affect the second and third copper layers very much. The vertical position of the copper atoms at the step-edges (Cu_S) is lower than that of the copper atoms (Cu_C) located between the copper atoms at the step-edge (Cu_S). The difference of z_{O1C} between the unreconstructed and reconstructed surfaces is 0.53 Å. This result indicates that the oxygen atoms move downward 0.53 Å towards the topmost copper surface in the missing row-reconstruction. This downward movement of the oxygen atom is consistent with previous *ab initio* calculations.[28] Based on this observation, the missing-row reconstruction makes the topmost copper layer move upward and the oxygen atoms move downward to get an energetically stable structure. This finding is consistent with what has been obtained in experiments.[11,18]

The structural parameters of the DFT-predicted missing-row reconstruction are compared to experimental results in Table 2. The distances between the second and third copper layer (z_{23}), the distance between the topmost copper atom at the step-edge and third copper layer (z_{1S3}), and the distance between the topmost copper atom (Cu_C) and third

copper layer (z_{1C3}) are comparable to the experimental results.[11,18] The vertical distance of an oxygen atom from a Cu_S atom (z_{O1S}) is overestimated with respect to the experiment, but that of the oxygen atom to Cu_C (z_{O1C}) is consistent with experimental results. Hence, the missing-row reconstruction structure predicted by DFT is comparable to the experimental results and we believe that the DFT method can be used for further investigation of the structural change in the proposed work.

3 Adsorption energy investigation of O_2 on a Cu(100) surface

The adsorption of oxygen on a copper surface is the first step in copper oxidation. Understanding the adsorption characteristics is important in the construction of an atomic-level model of copper oxidation. The purpose of the work presented in this section is to find the most favorable adsorption site on a Cu(100) surface. On the un-reconstructed Cu(100) surface, I calculated the adsorption energy for six different initial configuration of an oxygen molecule by varying the distance between oxygen atoms and the height from the topmost copper layer. The adsorption state for the minimum adsorption energy is compared to previous DFT calculation results. For the proposed work, the missing-row reconstruction will be investigated to find the most favorable adsorption site for an oxygen molecule because I believe that the further adsorption on the missing-row reconstruction is an important step in the transition from the missing-row reconstruction to the oxide island nucleation.

3.1 Computational detail

The Cu(100) surface that we used in our calculations is shown in Figs. 9(a) and 9(b). The $p(3\times3)$ unit cell is four layers deep (36 total atoms), and there is an 8 Å vacuum in the z-direction. Periodic boundary conditions (PBC) are applied in the x- and y-directions. There is no periodicity in the z-direction. The six potential adsorption sites defined by Alatalo *et al.*[38] have been investigated as shown at Figs. 9(a) and 9(b). The big spheres are copper atoms and small spheres are oxygen atoms. The arrows show the extent of the unit cell. To find the copper lattice constant, a bulk face centered cubic (fcc) structure was initially modeled with a $13\times13\times13$ k-point mesh. The zero-pressure bulk lattice constant is obtained by determining where the total system energy is minimized, as shown in Fig. 10(a). We obtain a value of 3.65 Å, which is slightly bigger than the experimentally measured value of 3.60 Å[63–65] but is consistent with previous DFT calculations.[38,66] The $p(3\times3)$ copper

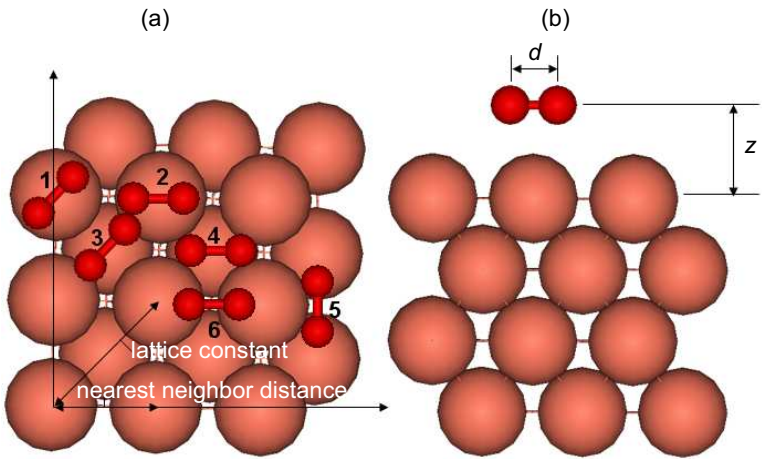

Figure 9: $p(3\times3)$ Cu(100) surface. The narrow lines between copper atoms are created by my visualization program and have no physical meaning. (a) Top view. Oxygen molecule adsorption sites: top sites (1-2), fcc sites (3-4) and bridge sites (5-6). (b) Side view. d is the bond length and z is the height between the center of mass of the oxygen molecule and the surface copper atoms.

surface structure is then built based on this lattice constant. The copper surface is first relaxed without the oxygen molecule. The relaxed structure is then used in single-point total system energy calculations with an oxygen molecule. To minimize the computational effort for the surface structure, we would like to use as coarse a k-point mesh as possible. The mesh must be fine enough, however, to predict mesh-independent results. To find a suitable mesh, k-point meshes between $1\times1\times1$ and $9\times9\times1$ were investigated for the surface structure, as shown in Fig. 10(b). As the number of k-points increases, the total system energy also increases and converges to -124.5 eV after the $3\times3\times1$ mesh. The energy difference between the $3\times3\times1$ and $9\times9\times1$ k-point mesh is 0.005 eV, and so the $3\times3\times1$ mesh is chosen for all single point energy calculation for the surface structure.

For the single point energy calculations, the distance between the two oxygen atoms (d) and the height (z) of the molecule from the copper surface are varied from 1.0 A to 2.4 A by 0.2 A increments. 1.21 Å is used for d instead of 1.2 Å because that is the oxygen bond length at equilibrium[67,68] measured by experiment. There are thus 64 (=8×8) calculations for each adsorption site and the total number of calculations is 384. The average time for each calculation is about 2.5 hours on single CPU. The oxygen molecule can be modeled in

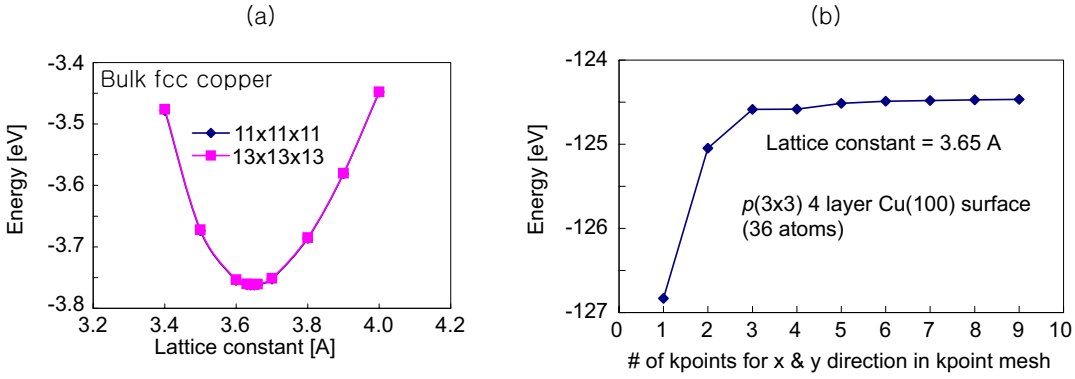

Figure 10: (a) Determining the optimized value for the bulk fcc lattice constant. (b) Finding the optimized number of k-points for the surface calculations.

a horizontal or vertical configuration. The horizontal configuration is shown in Figs. 9(a) and 9(b). In the vertical configuration, the molecular bond is perpendicular to the surface plane. In previous DFT calculations, the adsorption energy was investigated for both the horizontal and vertical configuration.[32,33,38] The horizontal configuration was found to be more energetically stable than the vertical configuration, and no dissociation was predicted in the vertical configuration. Therefore, only the horizontal configuration is studied in this work.

3.2 Preliminary results

The adsorption energy is calculated from[42]

$$E_{ads} = \frac{E_{O/Cu} - E_{Cu} - N_O \cdot \frac{E_{O_2}}{2}}{N_O}, \tag{1}$$

where $E_{O/Cu}$ is the total system energy of the oxygen-covered copper surface, E_{Cu} is the energy of the clean copper surface, E_{O_2} is the energy of an isolated oxygen molecule and N_O is the number of oxygen atoms in the computational cell. The minimum adsorption energy on each site is listed in Table 3. The adsorption energy is minimized when the oxygen

molecule (or its dissociated oxygen atoms) are adsorbed at a four-fold hollow site [see Figs. 11(a) for the adsorption of the dissociated oxygen atoms and Figs. 11(b) for the second lowest adsorption energy of the dissociated oxygen atoms]. The lowest adsorption energy is found at the bridge site (site 5) with $d = 2.4$ Å and $z = 1.0$ Å. This result is consistent with experiment[50] and previous DFT calculation.[38] The lowest adsorption energy is 0.31 eV lower than -1.68 eV calculated by Alatalo *et al.*,[38] who also found the four fold hollow site to be the most favorable adsorption site. We believe that this difference is a result of a differently sized computational cell (this information is not provided by Alatalo *et al.*[38]).

Site	d [Å]	z [Å]	E_{ads} [eV]
1	2.4	1.2	-1.16
2	2.4	1.2	-1.14
3	1.4	1.6	-1.06
4	1.6	1.4	-1.46
5	2.4	1.0	-1.99
6	1.4	1.8	-1.08

Table 3: The minimum adsorption energy and its associated distance (d) between the two oxygen atoms and height (z) above the copper surface. The sites are defined in Fig. 9

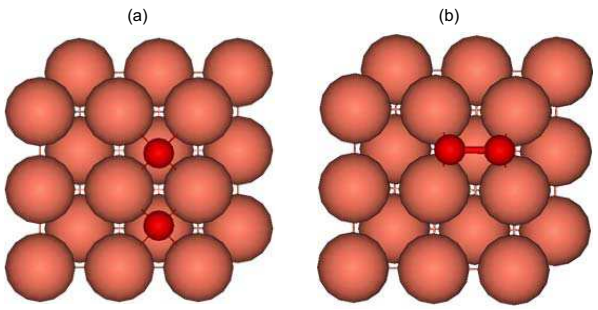

Figure 11: (a) Site 5 adsorption state. (b) Site 4 adsorption state. (See Table 3 for adsorption energy for each state.)

3.3 Proposed research

The missing-row reconstruction is the transition state from the clean copper surface to the copper (II) oxide island formation below 500 K.[48] The oxidation process requires more

oxygen atoms. As such, I believe that the missing-row reconstructed Cu(100) surface must still attract and dissociate oxygen molecules in order to supply atomic oxygen for further reconstruction or transformation into a copper (II) oxide island. To find the most favorable adsorption site on the missing-row reconstruction, I will apply DFT calculations for the four oxygen molecule configurations shown in Fig. 12. At this time, all oxygen atoms and copper surface will be fixed to investigate static energetics. For the single point energy calculations, the distance between the two oxygen atoms (d) and the height (z) of the molecule from the copper surface are varied and the total system energy will be calculated and the adsorption energy for each case will be calculated by Eq. 1. The findings of this investigation will be used for the investigation of the further oxygen-induced reconstruction on the missing-row reconstructed Cu(100) surface shown in Section 4.3.

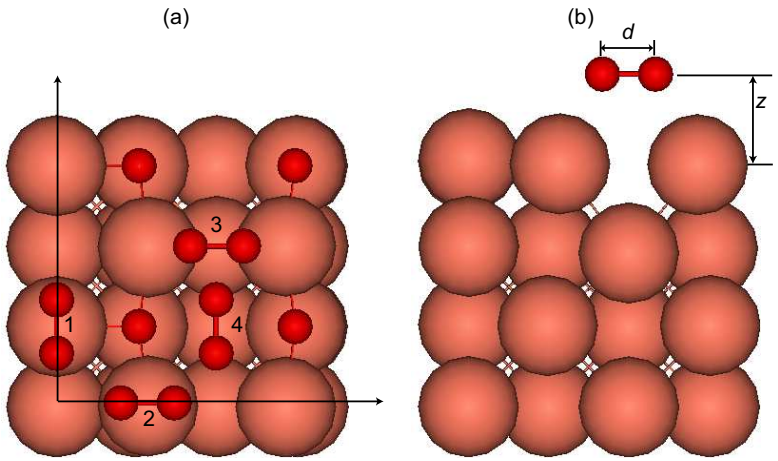

Figure 12: $p(2\sqrt{2}\times 2\sqrt{2})$ missing-row reconstructed Cu(100) surface. (a) Top view. Oxygen molecule adsorption sites: top sites (1-2) and missing-row sites (3-4). The arrows indicate the unit cell. (b) Side view. d is the bond length and z is the height between the center of mass of the oxygen molecule and the surface copper atoms.

4 Oxygen-induced reconstruction on a copper surface

The objective of this task is to identify the structural and energetic effects of placing an additional oxygen molecule on (or near) both the unreconstructed and reconstructed Cu(100) surfaces to investigate whether there is further surface reconstruction other than the missing-row reconstruction. The structural change and energetics of the surfaces with an additional oxygen molecule are investigated for different initial positions of the oxygen molecule and different unit cell sizes. There is no further reconstruction on the missing-row reconstructed Cu(100) surface based on current results. For the proposed work, I will modify the missing-row reconstruction by adding a point defect and investigate further oxygen-induced reconstruction on the surface. The Cu(110) surface will also be investigated for the oxygen-induced reconstruction.

4.1 Computational detail

For the unreconstructed Cu(100) surface at an oxygen coverage of 0.75 ML, Kangas *et al.*[42] found by DFT calculation that one of the three surface-adsorbed oxygen atoms moves down toward the topmost copper layer. I also found the same result in my DFT calculations. The relaxed surface structure is shown in Fig. 13. If there is another oxygen molecule above this lower oxygen atom, a repulsive interaction is expected between them and an attractive interaction is expected between the oxygen molecule and the topmost copper atoms because of the different electronegativaties of oxygen and copper.[69] The attractive and repulsive interactions are also found by Jaatinen *et al.*[46] through *ab initio* molecular dynamic simulation. The interactions might affect the structure and energetics of the Cu(100) surface. To specify the effect of the oxygen molecule on the oxygen adsorbed Cu(100) surface, structural relaxation is performed for both unreconstructed (oxygen coverage 0.75 and 1.0 ML) and reconstructed surfaces (oxygen coverage 0.5 ML). At the same time, different unit cell sizes are investigated to check for size effects. The different unit cells produce different distances

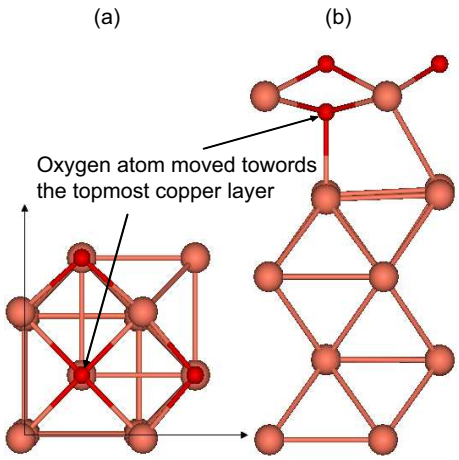

Figure 13: Relaxed Cu(100) surface structure at an oxygen coverage of 0.75 ML by DFT calculation. The bottom copper layer is fixed and the other copper and oxygen atoms are movable. (a) Top view. (b) Side view.

between the additional oxygen molecules (through the system periodicity).

In these calculations, the k-point mesh is 12×12×1 for the $p(1\times1)$ structure, 6×6×1 for the $p(2\times2)$ structure, and 3×3×1 for the $p(4\times4)$ structure. The bottom copper layer is fixed and all other atoms can move during the relaxation. Different initial positions of an oxygen molecule located 2 Å above the surface adsorbed oxygen atom are used, as shown in Fig. 14(a). The relaxed structures and adsorption energies will be discussed in Section 4.2. The $p(2\times2)$ and $p(4\times4)$ unit cell structures are investigated for an oxygen coverage of 0.75 ML. The $p(1\times1)$, $p(2\times2)$ and $p(4\times4)$ unit cells are investigated for an oxygen coverage of 1.0 ML. The $p(2\times2)$ and $p(4\times4)$ unit cell structures are shown in Figs. 15(a) and 15(b). In these two different unit cells, the distance between each oxygen molecule is different and I will compare the difference in terms of energetic and structural change.

For the reconstructed surface, the $p(2\sqrt{2}\times2\sqrt{2})$ unit cell is investigated using a k-point mesh of 8×8×1. The bottom copper layer is fixed and the other atoms can move. Structural relaxation is performed for different initial positions of an oxygen molecule located 1 Å above the topmost copper layer as shown in Fig. 14(b). The adsorption energy is calculated from Eq. (2) for the reconstructed surface. This equation is similar to Eq. (1), but modified for

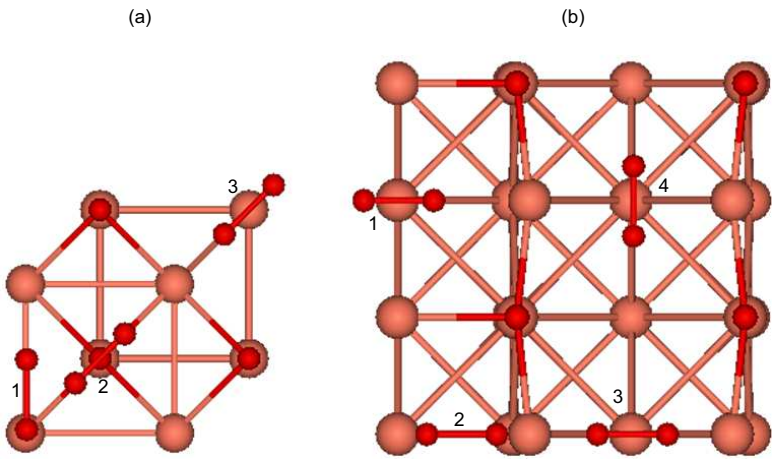

Figure 14: Initial positions of additional oxygen molecule. (a) $p(2\times2)$ at an oxygen coverage of 0.75 ML for the surface adsorbed oxygens. 1. Top-bridge site, 2. Fcc hollow site, and 3. Unoccupied fcc hollow site. (b) $p(2\sqrt{2}\times2\sqrt{2})$ missing-row reconstruction at an oxygen coverage of 0.5 ML for the surface adsorbed oxygens. 1. Fcc hollow site, 2. Middle point between the fcc hollow site and the copper atom at the step-edge, 3. Missing-row site with oxygen molecule perpendicular to the missing row, and 4. Oxygen molecule parallel to the missing row.

the missing-row reconstruction by

$$E_{ads} = \frac{E_{O/Cu_{rec}} - E_{Cu_{rec}} - (N_O - N_{O_{rec}}) \cdot \dfrac{E_{O_2}}{2}}{N_O - N_{O_{rec}}}. \tag{2}$$

Here, $E_{O/Cu_{rec}}$ is the total system energy of the oxygen molecule and missing-row reconstruction surface, $E_{Cu_{rec}}$ is the energy of the missing-row reconstruction surface and E_{O_2} is the energy of an oxygen molecule. N_O and $N_{O_{rec}}$ are the total number of oxygen atoms (including the oxygen molecule) and the total number of oxygen atoms on the reconstructed surface (excluding the oxygen molecule) in the computational cell. If Eq. (2) is applied to an unreconstructed surface, $N_{O_{rec}}$ is equal to zero and Eq. (2) reduces to Eq. (1).

4.2 Preliminary results

For the 0.75 ML coverage, the adsorption energies for each reconstructed surface are shown in Table 4 and the oxygen-induced reconstructions for position 2 are shown in Fig.

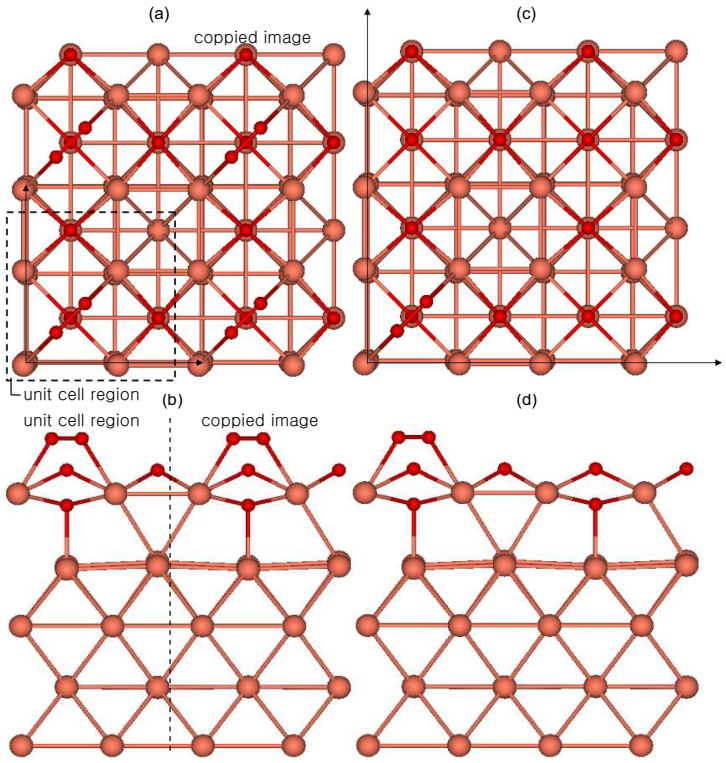

Figure 15: Unrelaxed Cu(100) at an oxygen coverage of 0.75 ML with additional oxygen molecule for different unit cell size [The $p(2\times2)$ unit cell is visualized to be compared to the p(4x4) unit cell. The atoms outside of the dashed line are copied from the atoms inside of the dashed line. The arrows indicate the unit cells.]; (a) Top and (b) Side view of the $p(2\times2)$ unit cell. (c) Top and (d) Side view of the $p(4\times4)$ unit cell.

16.

In the $p(2\times2)$ unit cell, elevated topmost copper atoms are predicted for all three initial positions of the additional oxygen molecule. As shown in Figs. 16(a) and 16(b) for position 2 of the oxygen molecule, two out of the four copper atoms in the topmost layer are elevated 1.34 Å above the un-elevated copper atoms. For positions 1 and 3, elevated copper atoms are also predicted and the vertical difference between the elevated and un-elevated copper atoms are 0.98 Å and 1.36 Å. The descended oxygen atom near to the topmost layer moves 0.05 Å upward for position 2 before and after relaxation, but it goes 0.15 Å downward in-between the topmost and the second layer for position 1 and 0.35 Å for position 3.

In the $p(4\times4)$ unit cell, a more complicated reconstruction is predicted. As shown in Figs. 16(c) and 16(d), there are elevated copper atoms. Two copper atoms, which are the nearest-

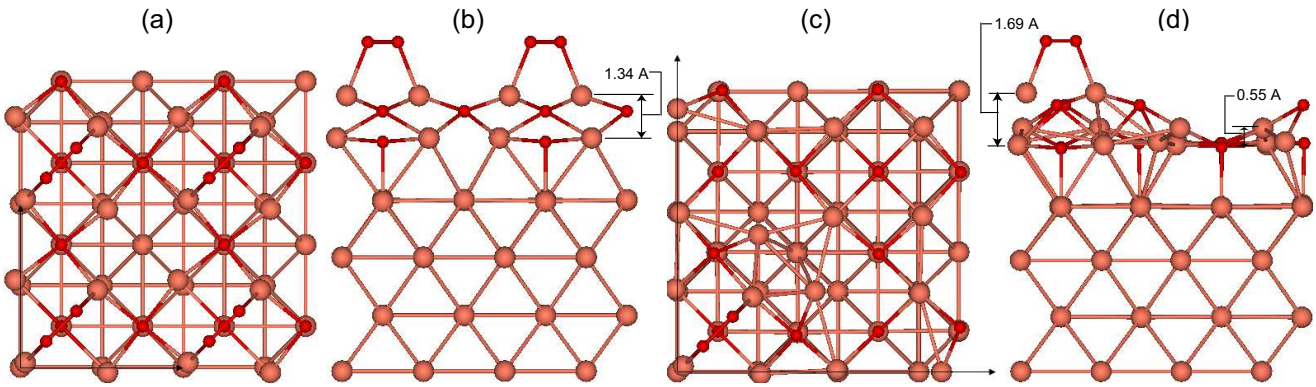

Figure 16: Oxygen-induced reconstruction on the Cu(100) surface at 0.75 ML coverage [see Fig. 14(a) for initial position of the oxygen molecule. The arrows indicate unit cell.]; (a) Top and (b) Side view of $p(2\times2)$ unit cell for position 2 (fcc hollow site). (c) Top and (d) Side view of $p(4\times4)$ unit cell for position 2.

	Adsorption energy [eV]		
unit cell	Position 1	Position 2	Position 3
$p(2\times2)$	-1.23	-1.27	-1.38
$p(4\times4)$	-1.24	-1.67	-1.67

Table 4: Adsorption energy for oxygen-induced reconstructions on the Cu(100) surface at 0.75 ML coverage [see Fig. 16 to match the adsorption energies shown here with their oxygen-induced reconstructions].

neighbors to the oxygen molecule, are elevated 1.24 Å for position 1, 1.69 Å for position 2, and 1.45 Å for position 3 above the un-elevated copper atoms in the topmost layer [see Fig. 16(d) for position 2]. The other elevated copper atoms move 0.77 Å for position 1, 0.55 Å for position 2, and 0.99 Å for position 3 above the un-elevated copper atoms. Note that the complicated reconstruction in the $p(4\times4)$ unit cell leads to a lower adsorption energy than the $p(2\times2)$ unit cell, as shown in Table 4.

For the 1.0 ML coverage, the oxygen-induced reconstructions on the Cu(100) surface are shown in Fig. 17 and the adsorption energies for each reconstructed surface are shown in Table 5. As shown in Fig. 17(a) and 17(a), there is no oxygen-induced reconstruction in the $p(1\times1)$ unit cell. As the unit cell size increases and amount of extra oxygen molecules decreases, however, there is stronger oxygen-induced reconstruction, as shown in Figs. 17(c)-17(f). The adsorption energy decreases as the unit cell size increases and the oxygen-induced

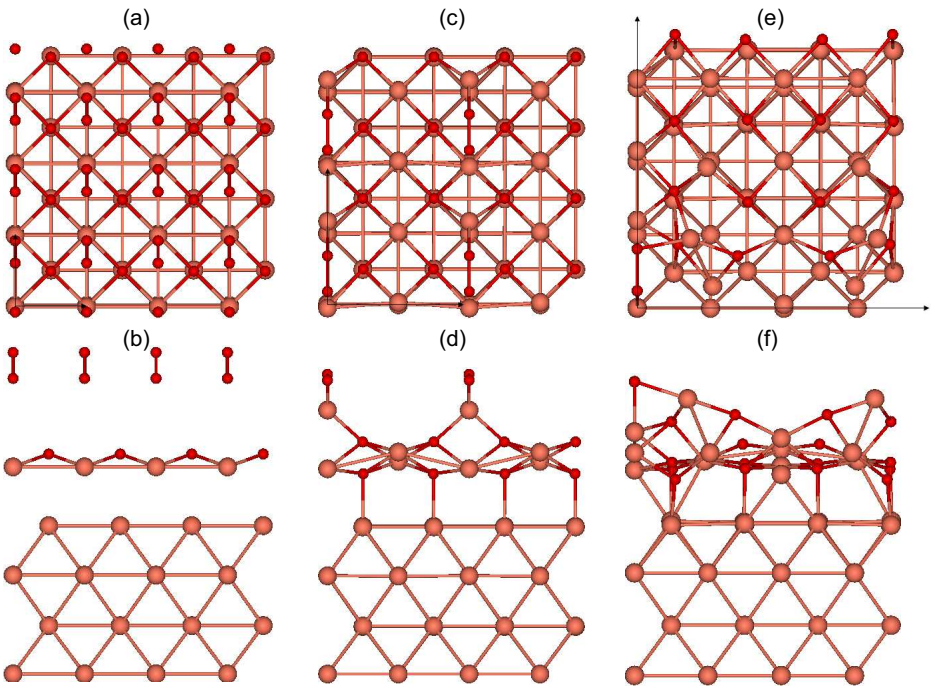

Figure 17: Oxygen-induced reconstruction on the Cu(100) surface at 1.0 ML coverage [see Fig. 14(a) for initial position of the oxygen molecule. The arrows indicate unit cell.]; (a) Top and (b) Side view of $p(1\times1)$ unit cell for position 1 (top-bridge site). (c) Top and (d) Side view of $p(2\times2)$ unit cell for position 1. (e) Top and (f) Side view of $p(4\times4)$ unit cell for position 1.

reconstruction appears more strongly, as shown in Table 5. An artificial periodicity is imposed by DFT calculation and the effect is stronger in a small unit cell than the big unit cell. The periodicity is essential for DFT calculation but we need big enough unit cell size to get more realistic predictions.

As we see in the results for the 0.75 ML and 1.0 ML coverage cases, the oxygen-induced reconstruction (*i.e.* elevation of the topmost copper atoms) makes an energetically more favorable reconstructed structure. The reconstruction is predicted, if the unit cell size is big enough to decrease the effect of an artificial periodicity imposed by DFT calculation.

For the missing-row reconstruction at 0.5 ML coverage, the oxygen-induced structural changes and the adsorption energies on the missing-row reconstructed Cu(100) surface are shown in Fig. 18 and Table 6 for different initial positions of oxygen molecule. In the missing-row reconstructed Cu(100) surface, there is not a big structural change, as I found for the

	Adsorption energy [eV]	
unit cell	Position 1	Position 2
$p(1\times1)$	-0.59	-0.29
$p(2\times2)$	-1.35	-1.05
$p(4\times4)$	-1.71	-1.71

Table 5: Adsorption energy for oxygen-induced reconstructions on the Cu(100) surface at 1.0 ML coverage [see Fig. 17 to match the adsorption energies shown here with their oxygen-induced reconstructions].

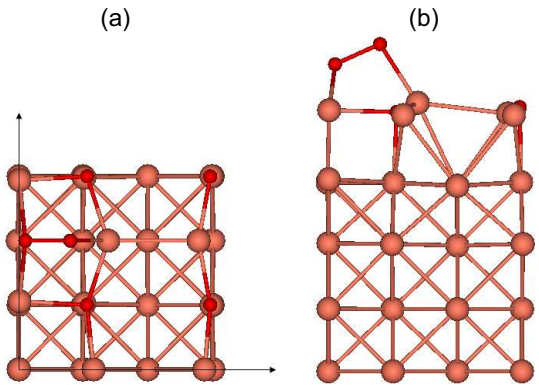

Figure 18: Oxygen-induced structural change on the missing-row reconstruction of the Cu(100) surface at 0.5 ML coverage [see Fig. 14(b) for initial position of the oxygen molecule. The arrows indicate $p(2\sqrt{2}\times2\sqrt{2})$ unit cell.]; (a) Top view for position 2 (middle-point between the fcc hollow site and the copper atom at the step-edge). (b) Side view for position 2.

cases of unreconstructed Cu(100) at 0.75 ML and 1.0 ML coverage. If the oxygen molecule is located near the step-edge copper atom (position 2), as shown in Figs. 18(a) and 18(b), it elevates the nearest neighbor copper atom at the step-edge by 0.30 Å and the adsorption energy is 0.30 eV less than at the fcc hollow site (position 1). The lower adsorption energy indicates that position 2 is energetically more stable than position 1. If the oxygen molecule

	Adsorption energy [eV]			
unit cell	Position 1	Position 2	Position 3	Position 4
$p(2\sqrt{2}\times2\sqrt{2})$	-0.27	-0.57	-0.48	-0.11

Table 6: Adsorption energy for oxygen-induced structural change on the missing-row reconstruction of Cu(100) surface at 0.5 ML coverage.

is located initially at the missing row site, the step-edge copper atoms are elevated by 0.23 Å for position 3 and there is no elevation for position 4.

Based on these structural and energetic changes, the additional oxygen molecule does change the unreconstructed Cu(100) surface significantly but it does not affect the missing-row reconstructed Cu(100) surface significantly. This indicates that the missing-row reconstruction is a much more stable structure than the unreconstructed surface, as found in experimental results. To find transition structure of missing-row reconstruction to copper (II) oxide island nucleation, a point defect and a bigger unit cell for the missing-row reconstructed Cu(100) surface will be investigated.

4.3 Proposed research

4.3.1 Oxygen-induced reconstruction on the missing-row reconstructed Cu(100) surface

To explore further oxygen-induced reconstruction on the missing-row reconstruction of the Cu(100) surface, I will add a point defect to the missing-row reconstructed surface. The initial positions of the point defect are shown in Fig. 19. For example, a copper atom at a

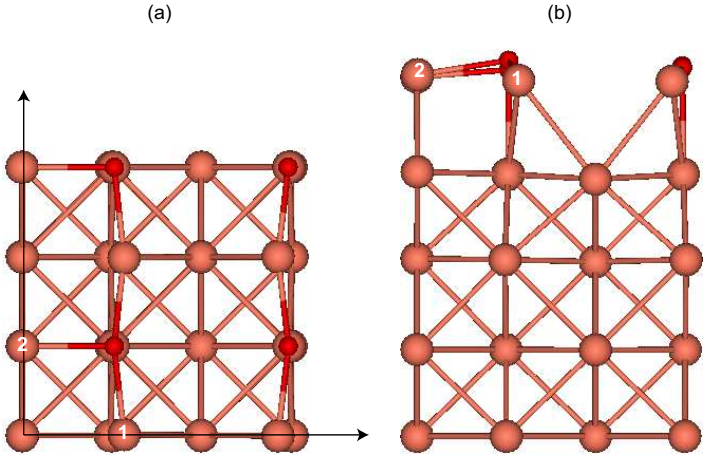

Figure 19: Initial positions of a point defect in the $p(2\sqrt{2} \times 2\sqrt{2})$ missing-row reconstruction on the Cu(100) surface at an oxygen coverage of 0.5 ML. (a) Top view. 1. Copper atom at a step-edge (Cu_S). 2. Copper atom located between the copper atoms at the step-edges (Cu_C).

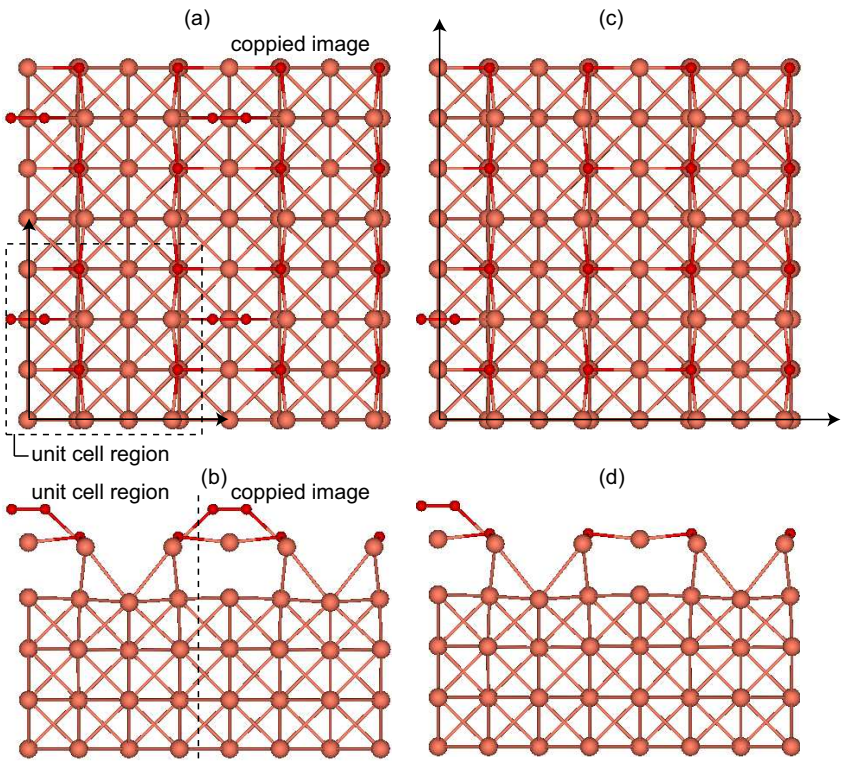

Figure 20: Unrelaxed missing-row reconstruction on the Cu(100) at an oxygen coverage of 0.5 ML with additional oxygen molecule for different unit cell size [$p(2\sqrt{2}\times2\sqrt{2})$ structure is visualized to be compared to $p(4\sqrt{2}\times4\sqrt{2})$ structure. The atoms outside of the dashed line are copied from the atoms inside of the dashed line. The arrows indicate the unit cells.]; (a) Top and (b) Side view of the $p(2\sqrt{2}\times2\sqrt{2})$ unit cell. (c) Top and (d) Side view of $p(4\sqrt{2}\times4\sqrt{2})$ unit cell.

step-edge (Cu_S) will be removed from the $p(2\sqrt{2}\times2\sqrt{2})$ unit cell, and an oxygen molecule is added to the initial positions shown in Fig. 14(b). The total system will then be relaxed. For the two initial positions of a point defect, four different initial positions of an oxygen molecule will be considered. The adsorption energy will also be calculated. Additional initial position for an oxygen molecule will be applied based on the adsorption energy investigation for the missing-row reconstruction proposed in Section 3.3.

To predict the oxygen-induced reconstruction, as shown in Fig. 17, a big enough unit cell size is required to remove the effects of artificial periodicity. In the preliminary investigation, I only used the $p(2\sqrt{2}\times2\sqrt{2})$ unit cell to predict the oxygen-induced reconstruction on the missing-row reconstructed Cu(100) surface. I now believe that this unit cell size was not big

enough to remove the effect of artificial periodicity. To test this hypothesis, the $p(4\sqrt{2}\times4\sqrt{2})$ unit cell will be relaxed with an additional oxygen molecule, as shown in Fig. 20. After the relaxation, the structural and energetic changes will be investigated.

4.3.2 Oxygen-induced reconstruction on the Cu(110)

The Cu(110) surface displays different adsorption and reconstruction phenomena compared to the Cu(100) surface, as observed by experiments[6,7,17,20,70,71] and as predicted by DFT calculation.[30,32,72,73] For example, the oxygen adsorption sites [see Figs. 21(a) and 21(c)] are very different with respect to the Cu(100) surface. This difference affects the energetics of oxygen adsorption and the oxygen-induced surface reconstruction on the Cu(110) surface. For the Cu(110) surface, the most stable adsorption site is the long bridge site (lb) for atomic oxygen[30] and the four-fold hollow site for the molecular oxygen[32] predicted by DFT calculation.

Jensen *et al.*[70] found the added-row reconstruction on Cu(110) by STM, as shown in Fig. 22. Kuk *et al.*[71] explained the mechanism for the transition from the added-row to

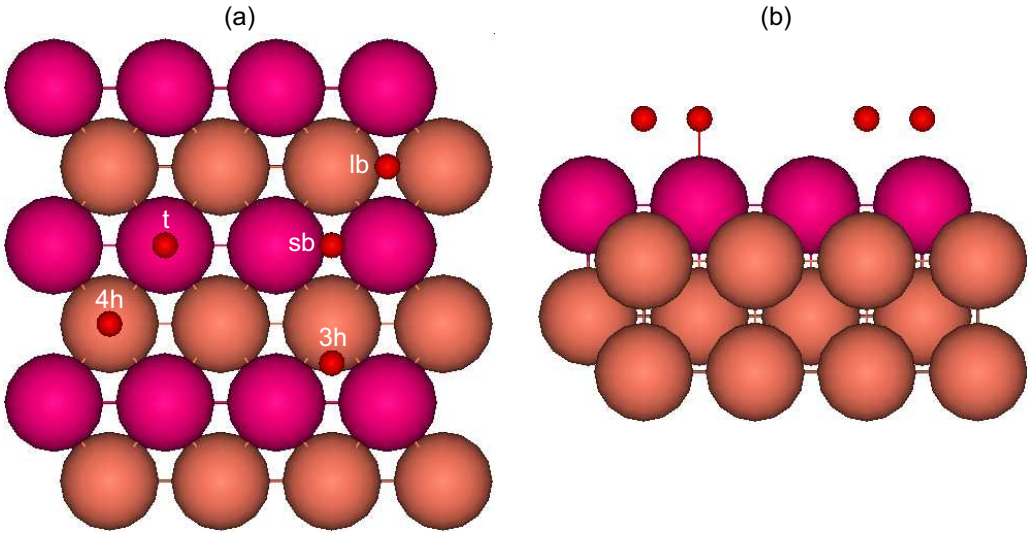

Figure 21: (a) Adsorption sites on the Cu(110) surface (3h: three-fold hollow site, 4h: four-fold hollow site, t: top site, sb: short bridge site, lb: long bridge site). (b) Side view of the Cu(110) surface. The topmost copper layer is colored differently. The oxygen adsorption sites are from Pang *et al.*[73]

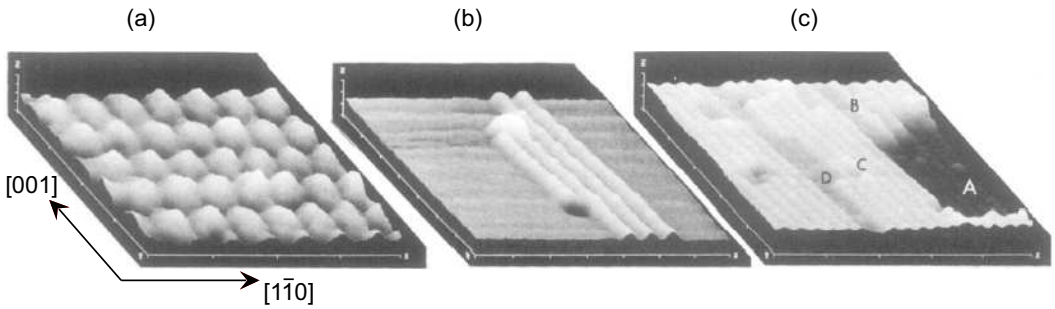

Figure 22: STM images on Cu(110) surface; (a) Cu(110) bare surface (20×20 Å^2 region and 0.16 Å/division for the z scale). (b) The formation of added-row reconstruction (70×70 Å^2 region and 0.8 Å/division for the z scale). (c) Missing-row reconstruction [Cu(110)-O(2×1) phase, In Fig. 22(c), there are several types of defects or irregularities. (A: one atomic layer descended missing-row reconstruction terrace, B: a shifted single chain of copper and oxygen atoms, C: a point defect (vacancy), D: $c(6\times2)$ reconstructed terrace, which is 0.4 Å lower than the missing-row reconstruction terrace.] (100×100 Å^2 region and 0.8 Å/division for the z scale).

the missing-row reconstruction, which is the saturated oxygen covered reconstruction of the added-row model on the Cu(110) surface, as shown in Fig. 23. According to Kuk *et al.*, a diffusing copper atom moves along [1$\bar{1}$0] direction [see Figs. 23(a), and 23(b)], the copper atom is bound to the diffusing oxygen atoms, and then the oxygen atoms are adsorbed in the preferred long bridge site. This reaction is repeated and then the Cu(110) surface is reconstructed as the missing-row reconstruction at the saturated oxygen covereage [see Fig. 22(c), and 22(d)]. By DFT calculation, it is found that the added-row and missing-row reconstruction makes the Cu(110) surface energetically more stable than unreconstructed surface.[30] If more oxygen atoms are supplied to the reconstructed Cu(110) surface, the copper oxide is formed and grown horizontally and vertically, as observed by STM.[6,7] To find a specific model from the transition from the missing-row reconstruction to the copper oxide formation, I will investigate the further oxygen-induced reconstruction on the missing-row reconstructed Cu(110) surface at the saturated oxygen coverage by DFT calculation. In the relaxed added-row (less saturated oxygen coverage) and missing-row (saturated oxygen coverage) reconstruction, I will put an additional oxygen molecule and relax the copper surface with the oxygen molecule, as I did for the Cu(100) surface previously. The structural

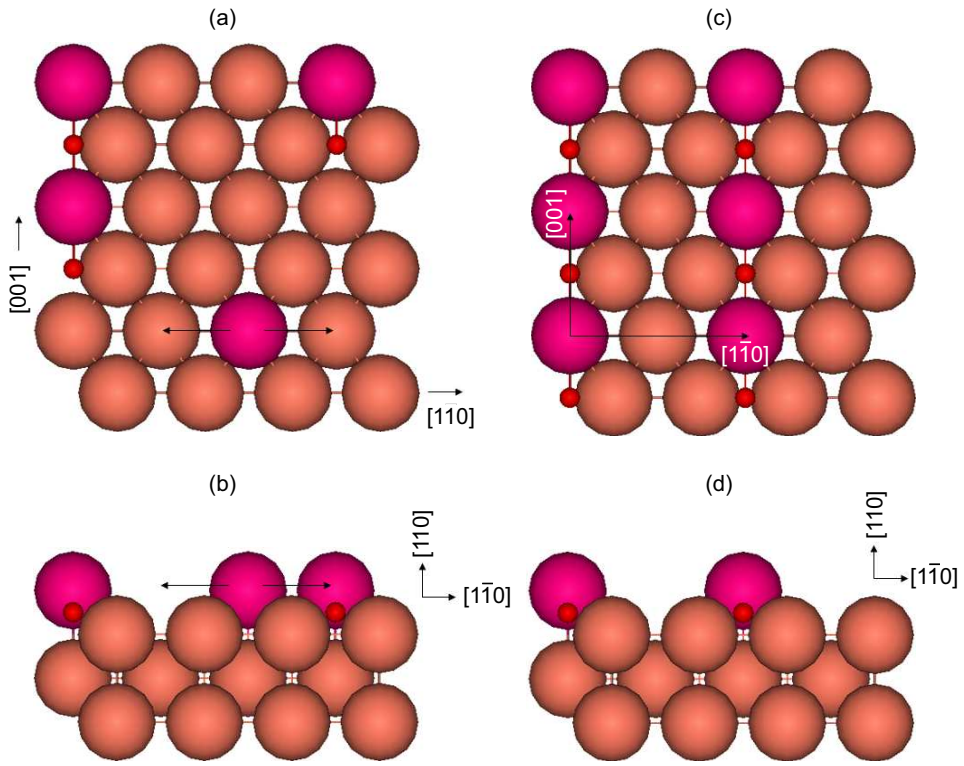

Figure 23: Oxygen-induced reconstruction on Cu(110) surface; (a) Top and (b) Side view of added-row reconstruction (The arrows of the topmost copper atom indicate the copper diffusion direction). (c) Top and (d) Side view of missing-row reconstruction.

and energetic change will be investigated for different oxygen coverages and unit cell sizes.

As shown in Fig. 22(c), there are defects and irregularities on the real Cu(110) surface. The defects will affect the oxide formation and growth.[7] For this reason, I will apply point defect (vacancy) or line defect (dislocation) to the Cu(110) surfaces and compare them to the perfect (defect-free) cases structurally and energetically.

5 Energetics of embedding oxygen atoms into a copper surface

The purpose of the work described and presented in this section is to investigate the relationship between the energy barrier for embedding an oxygen atom into a Cu(100) surface and the oxygen coverage and surface morphology. I found that the energy barrier decreases as the oxygen coverage increases in the $p(2\times2)$ unit cell for the unreconstructed Cu(100) surface. Structural changes by an oxygen embedment and electron density of state (DOS) for the embedding oxygen atom and copper atoms in the top and second layer are investigated. For the missing-row reconstructed Cu(100) surface, I did not find an energetically favorable site between the top and second copper layer for an embedding oxygen atom. For the proposed work, other oxygen embedment paths and additional oxygens will be applied to find the relationship between the energy barrier and the oxygen coverage/morphology.

5.1 Surface diffusion and oxygen embedment into a copper surface

During oxide islands formation and growth on a copper surface, the oxide grows parallel and into the copper surface [as observed by ultra high vacuum (UHV)-TEM[7]]. Surface diffusion (of oxygen and copper atoms) is the key mechanism for oxide island formation and has been observed experimently.[5,8,23] During a diffusion event, an atom (or molecule) starts and ends in thermodynamically favorable states that are separated by an energy barrier. The energy barrier is the energy difference between the initial state and the local maxima state along the minimum energy path (MEP, note that the energy barrier is path-dependent). The nudged elastic band (NEB) method is a computational approach for finding the MEP between specified initial and final states.[74] To find the MEP, a set of images (typically 4-20) is created between the given initial and final states.[75] The images are connected by virtual springs. During the iterative calculation procedure, each image is relaxed while interacting with the adjacent images. To validate my NEB calculation approach, I applied the NEB

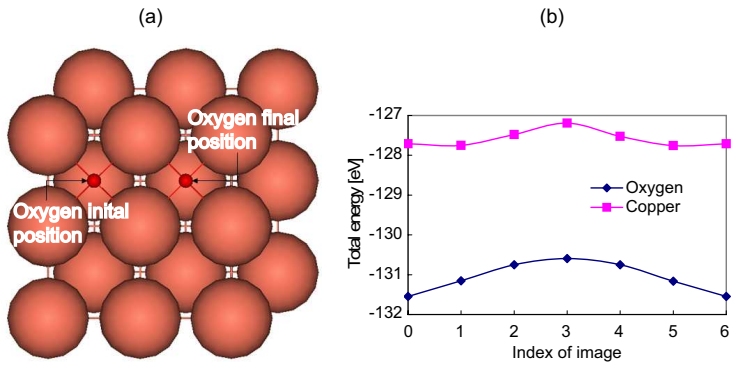

Figure 24: (a) A set of images for the NEB method for horizontal diffusion on the Cu(100) surface. (b) Index of image vs. total system energy from NEB method calculation for horizontal diffusion of copper and oxygen atom on Cu(100) surface.

Diffused atom	Energy barrier [eV]	Ref[38] [eV]
Oxygen	0.95	0.74
Copper	0.56	0.53

Table 7: Energy barrier calculated by NEB for atomic oxygen and copper diffusion on Cu(100) surface.

method to calculate the energy barrier for the diffusion of atomic oxygen and copper on the Cu(100) surface. As shown in Fig. 24(a), the inital and final positions are four-fold hollow site on the Cu(100) surface. The calculation results are shown in Fig. 24(b) and Table 7. Our calculated energy barrier is 6.5% larger for atomic copper diffusion and 28.6% larger for atomic oxygen diffusion than a previously reported calculation.[38] In that work, the size of their unit cell, the details on the pseudo-potentials, and the total number of images used are not specified, which may explain the differences. The results are all less than 1 eV, typical values for surface diffusion.[38,76]

To explore the energetics of oxide embedding into a copper surface, which has not previously been examined, we performed NEB calculations. The detailed computational set-up and result are presented in section 5.2 and 5.3.

5.2 Computational detail

For the NEB calculations, spin-polarized calculations are used and the energy cut-off value is 330 eV. Spin-polarization is required for NEB calculation[77] and 330 eV is chosen as a trade-off between computational efficiency and accuracy. 6×6×1 and 8×8×1 k-point meshes are used for the $p(2\times2)$ and $p(2\sqrt{2}\times2\sqrt{2})$ unit cells.

As Kangas *et al.*[42] found, the adsorption energy for the Cu(100) surface varies with on- and sub-surface oxygen coverage. To investigate the relationship between surface energetics and oxygen coverage, I applied the NEB method is applied to the $p(2\times2)$ surface structure at 0.25 ML, 0.5 ML, 0.75 ML, and 1.0 ML coverages. The $p(2\times2)$ unit cell has five copper layers and the bottom copper layer is fixed.

In addition, it is also important to consider the surface morphology. There are three possible surface structures for an oxygen coverage of 0.5 ML: (i) $c(2\times2)$, (ii) missing-row reconstruction, and (iii) $c(2\times2)$ with 0.25 ML disordered vacancy. To investigate the relationship between the energetics and surface morphology, I also applied the NEB method to the different surface structures with an oxygen coverage of 0.5 ML. The $p(2\sqrt{2}\times2\sqrt{2})$ unit cell, including three copper layers with the bottom layer fixed, is chosen for this investigation. We initially relaxed a $p(2\sqrt{2}\times2\sqrt{2})$ unit cell with five layers and found that there is no change in the two bottom layers. To get a reasonable computational load, the bottom two layers were then removed.

To determine the approximate location of an embedded oxygen atom, single-point energy calculations were performed to relax the $p(2\times2)$ unit cell at an oxygen coverage of 0.25 ML at fixed vertical positions of the oxygen atom. For each single-point energy calculation, the vertical position of oxygen is decreased by 0.285 Å from the position of the relaxed surface-adsorbed oxygen until the mid-point between the top and second copper layers is reached. The calculated total system energy and relaxed structures are shown in Fig. 25.

Fig. 25(a) shows that there is a relatively big increase of total system energy between 6.6 Å and 6.3 Å. At 6.3 Å, there is a physically non-reasonable movement of a copper atom

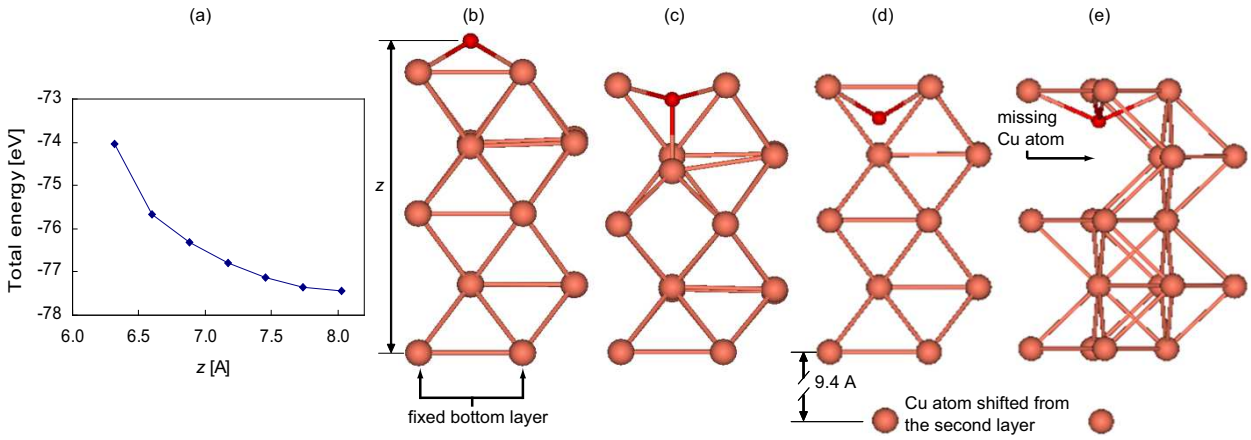

Figure 25: (a) Vertical position of oxygen atom (z) vs. total system energy plot for $p(2\times2)$ unit cell at an oxygen coverage of 0.25 ML. (b) Relaxed structure of oxygen at 8.025 Å. (c) Relaxed structure of oxygen at 6.599 Å. (d) Relaxed structure of oxygen at 6.314 Å. (e) Rotated view of relaxed structure of oxygen at 6.314 Å. [Figs. 25(d) and 25(e) show the physically unreasonable offset of copper atom.]

from the second layer to 9.4 Å beneath the fixed bottom layer as shown in Figs. 25(d) and 25(e). Therefore, the minimum vertical position of an embedding oxygen atom must be bigger than the middle point between the topmost and second copper layer (6.314 Å) to prevent a physically unreasonable relaxed structure. In this work, 6.7525 Å is chosen for the minimum vertical position for an embedding oxygen atom for all NEB calculations.

To find the relaxed initial and final states, single-point energy calculations are performed. Then, the intermediate images are created. Five images are applied for the $p(2\times2)$ unit cell and four images are applied for the $p(2\sqrt{2}\times2\sqrt{2})$ unit cell, as it is a bigger structure and more computationally demanding. The sets of images, oxygen initial position, and oxygen final position are shown in Figs. 26(a) and 26(b) for the $p(2\times2)$ unit cell and Figs. 26(c) and 26(d) for the $p(2\sqrt{2}\times2\sqrt{2})$ unit cell. For the oxygen atom embedding path, the relaxed oxygen position at the initial state is used as a starting point, and the same minimum vertical position at final state (6.7525 Å from the fixed bottom copper layer) is used for each of the calculations.

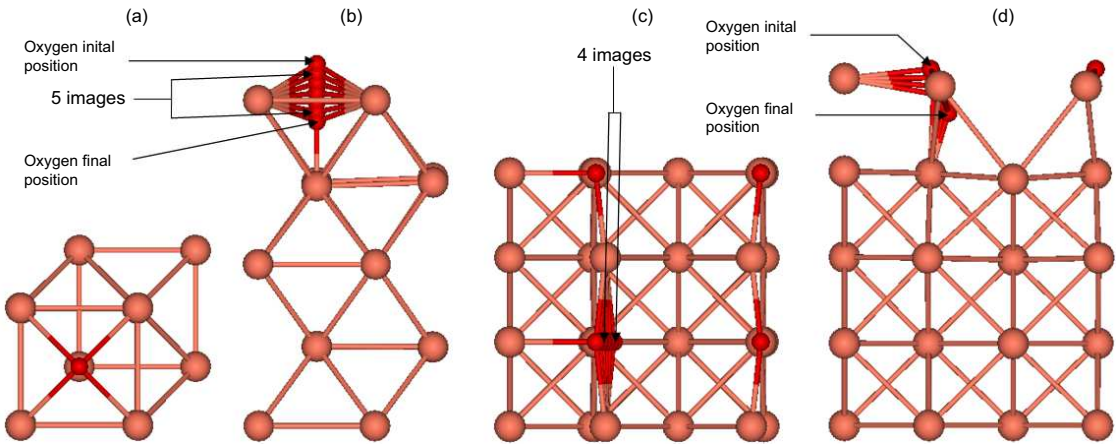

Figure 26: (a) Top and (b) Side view of $p(2\times2)$ unit cell at 0.25 ML coverage with five images for NEB calculation. (c) Top and (d) Side view of $p(2\sqrt{2}\times2\sqrt{2})$ unit cell at 0.5 ML coverage with four images for NEB calculation.

5.3 Preliminary results

The NEB method results for the $p(2\times2)$ unit cell are shown in Fig. 27(a). As the surface-adsorbed oxygen atom moves toward the topmost copper layer, the surface changes structurally and energetically. The total system energy of the system increases because it is moving away from a stable state. For example, as shown in Fig. 27(a), the total system energy of the 0.25 ML $p(2\times2)$ system increases when the vertical position of oxygen atom decreases. The monotonic energy increase indicates that the embedding oxygen atom always makes the copper surface energetically unstable.

For the other oxygen coverage cases, the energy difference between the initial and final states decreases as the oxygen coverage increases, as shown in Fig. 27(a) and Table 8. In Figs. 27(a) (coverage of 0.75 ML and 1.0 ML), a local maxima and minima of the total system energy is found. For the embedding oxygen to go to the local minima state (image 4) on the Cu(100) surface at 0.75 ML oxygen coverage, it must overcome the energy difference between initial state and the local maxima. The corresponding energy difference is the energy barrier. The energy barrier decreases with increasing oxygen coverage as shown in Table 8. The oxygen atom can embed into the copper surface more easily at 1.0 ML coverage than 0.75 ML coverage. For 1.0 ML coverage, the total system energy decreases. The negative

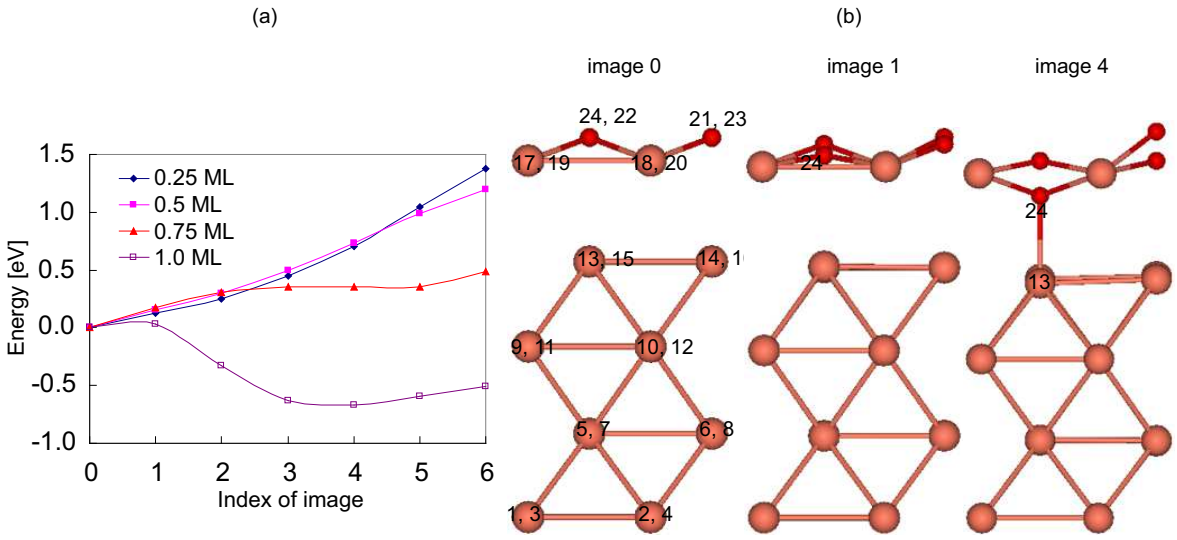

Figure 27: (a) Total system energy in each image predicted by NEB calculation for different oxygen coverage in the $p(2\times2)$ unit cell. The energy value is shifted by the energy of image 0 (energy of each image - energy of image 0). The step size between adjacent images is 0.25 Å for 0.75 ML coverage and 0.21 Å for others because the oxygen atom is elevated from the topmost surface in 0.75 ML coverage, the embedding depth is fixed and the step size is bigger than other cases. (b) Transition structure of image 0, image 1, and image 4 at an oxygen coverage of 1.0 ML. The atomic labels in the transition structures are used for index numbers for electron density of state (DOS) calculation among oxygen and copper atoms in Figs. 29, and 30.

energy difference indicates that the embedded oxygen atom makes the system energetically more stable. More discussion about the 1.0 ML coverage is provided later in this section.

The structural change for the different coverages is investigated by comparing the vertical position of the topmost copper layer to the embedding oxygen atom in the transition structures, as shown in Fig. 28. For coverages of 0.25 ML and 0.5 ML [Figs. 28(a) and 28(b)], both the embedding oxygen atom and the topmost copper layer move downward. At a certain point (image 5 for 0.25 ML and image 4 for 0.5 ML), the oxygen atom moves beneath the topmost copper layer. For the 0.75 ML coverage, as shown in Fig. 28(c), the oxygen atom and the topmost copper layer initially both move downward. A similar trend is observed for the 1.0 ML coverage, as shown in Fig. 28(d). As shown in Figs. 28(a), 28(b), 28(c), and 28(d), the vertical position of the topmost copper layer increases as the oxygen coverage increases. This result indicates that while the embedding oxygen atom causes the topmost

Oxygen coverage	0.25 ML	0.5 ML	0.75 ML	1.0 ML
Energy difference [eV]	1.383	1.199	0.243	-0.505
Energy barrier [eV]	-	-	0.285	0.035

Table 8: Energy difference and energy barrier calculated by NEB for an oxygen embedment in $p(2\times2)$ unit cell of Cu(100) surface with different oxygen coverage; Energy difference is calculated by subtracting the total system energy of image 0 (initial state) from that of image 6 (final state). The energy barrier is the energy difference between initial state and the state of local energy maxima.

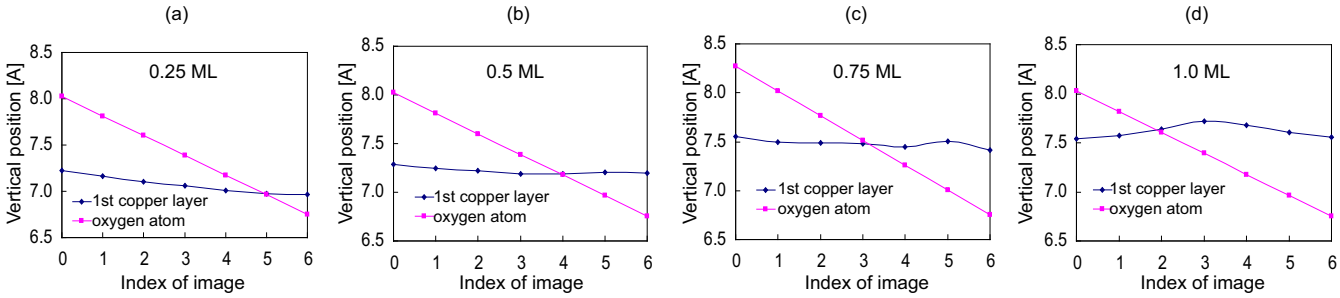

Figure 28: Comparison of vertical position between the topmost (1^{st}) copper layer and the embedding oxygen atom for different oxygen coverage (The oxygen coverage is shown in each plot.); In case of high oxygen coverage (0.75 ML and 1.0 ML), the topmost copper layer downward movement is less than low oxygen coverage cases (0.25 ML and 0.5 ML). In each case, there is only one oxygen atom embedding into copper surface and more surface-adsorbed oxygen atoms stays on-surface four-fold hollow site in high oxygen coverage than low oxygen coverage cases and those surface-adsorbed oxygen atoms weaken the embedding oxygen atom effect for the downward movement of the topmost copper layer.

copper layer to move downward, the other surface-adsorbed oxygen atoms, which maintain their on-surface four-fold hollow sites, provide an opposing force. As the oxygen coverage increases, the number of surface-adsorbed oxygen atoms maintaining their on-surface four-fold hollow sites also increases, and their effect increases. This phenomenon explains why the embedding oxygen can penetrate the topmost copper layer more easily at higher oxygen coverages.

To further explore the changes in structure and energetics as the oxygen coverage increases, the local electron density of state (DOS) is calculated from the initial, final, and transition structures, as shown in Fig. 29. In Fig. 29(a), there are two peaks at -6.304 eV. This indicates that there is a higher electron density at -6.304 eV than at any other energy

level in both the d-orbital of the topmost copper atom and the p-orbital of the embedded oxygen atom. This is the hybridization between the p-orbital of oxygen and the d-orbital of copper atom (p-d hybridization), which, as shown by Stolbov *et al.*,[34] is a typical sign of a strong interaction. The p-d hybridization is predicted in other DFT calculations for the oxygen adsorption on unreconstructed and reconstructed Cu(100) surfaces,[34,38,43] and on Cu(111) surfaces.[33]

In Figs. 29(a), 29(b), 29(c), and 29(d), which show the initial state with increasing oxygen coverage, the p-d hybridization grows stronger. A stronger p-d hybridization is predicted for higher oxygen coverage after the oxygen embedment as shown in Figs. 29(e), 29(f), 29(g), and 29(h). Comparing Fig. 29(a) and 29(e), however, it is seen that the hybridization between the embedding oxygen atom and the topmost copper atom weakens after the oxygen embedment and this trend is found for all other oxygen coverage cases. Consistent with the findings of Stolbov *et al*,[34] the oxygen embedment increases the atomic spacing between the embedding oxygen and the copper atom in the topmost layer, and weakens the p-d hybridization. Based on these predictions, the oxygen embedment weakens the p-d hybridization between the embedding oxygen atom and the copper atom in the topmost layer, and the relative difference between before and after the oxygen embedment grows bigger along increasing oxygen coverage.

For 1.0 ML coverage, as discussed previously, the energetics is inverted (*i.e.* the energy difference between the initial and final states is negative), as shown in Fig. 27(a) and Table 8. For 1.0 ML coverage, if one of the four surface-adsorbed oxygen atoms is embedding into the copper surface and it is located between the topmost and second copper layer as shown in Fig. 27(b), the entire system gets energetically more stable than the case of four surface-adsorbed oxygen atoms on the copper surface. The energy barrier is only 0.035 eV ($= 5.37 \times 10^{-21}$J) and if an oxygen atom has enough kinetic energy, it can overcome this energy barrier without any extra driving force. To investigate the oxygen embedding from the viewpoint of electronic structure, the DOS is calculated for the p-orbital of the embedding

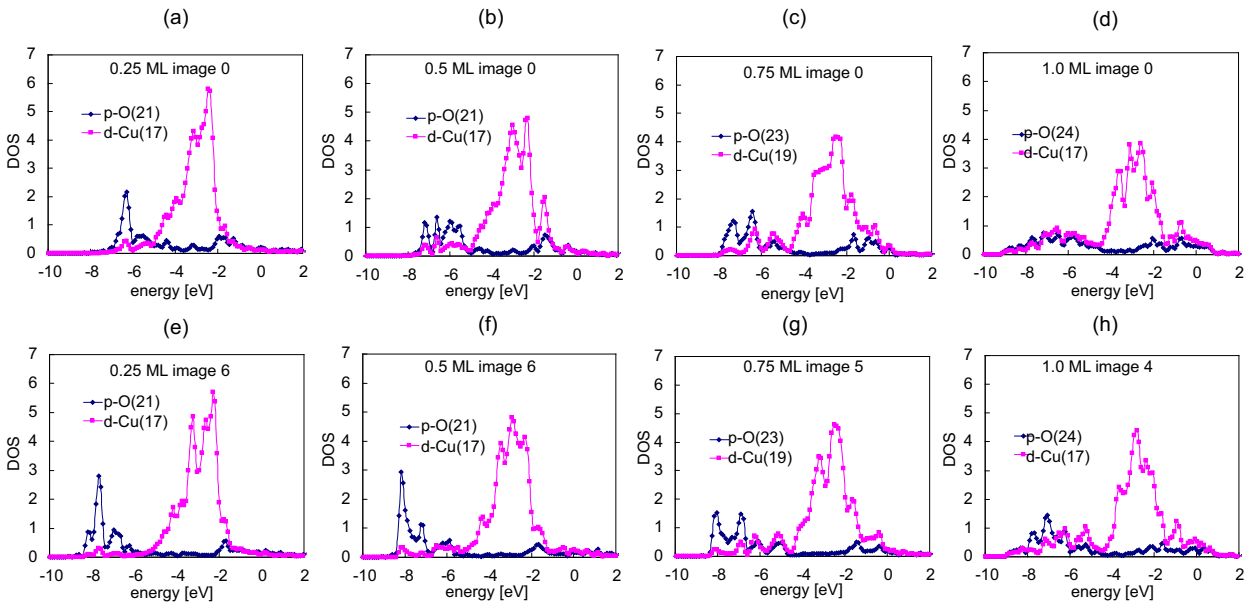

Figure 29: Comparison of DOS between p-orbital of oxygen atom [p-O(index number)] and d-orbital of copper atom [d-Cu(index number)] in the transition structures of $p(2\times2)$ surface structure. The index numbers of copper atoms are shown in Fig. 27(b) and O(21), O(23), and O(24) are the embedding oxygen atoms in each oxygen coverage.; The oxygen coverage of each surface structure increases as you go from left to right in each row of plots of Fig. 29. These DOS results show the comparison between the embedding oxygen atom and its nearest neighboring copper atom in the topmost copper layer before [from Fig. 29(a) to 29(d)] and after [from Fig. 29(e) to 29(h)] the oxygen atom embedding into the copper surfaces, which have different oxygen coverage.

oxygen and the d-orbital of the copper atoms in the topmost and second layers from the transition structures of image 0, image 1 (local energy maxima), and image 4 (local energy minima) as shown in Fig. 30. There is a strong p-d hybridization between the embedding oxygen and the copper atom in the topmost layer [see Fig. 30(a)], the p-d hybridization is disordered and weakened by embedding the oxygen into copper surface [see Fig. 30(b)], and is relatively weak [see Fig. 30(c)] at the energetically stable oxygen position. In the second copper layer, there is no p-d hybridization with the embedding oxygen atom in the initial state [see Fig. 30(d)], but a relatively weak p-d hybridization develops between -2 eV and 2 eV [see Figs. 30(e) and 30(f)] as the oxygen atom embeds. For the topmost copper layer, the d-orbitals of the copper atoms are exactly the same in image 0, as shown in Fig. 30(g). As oxygen is embedding into the copper surface, however, the d-orbitals are slightly

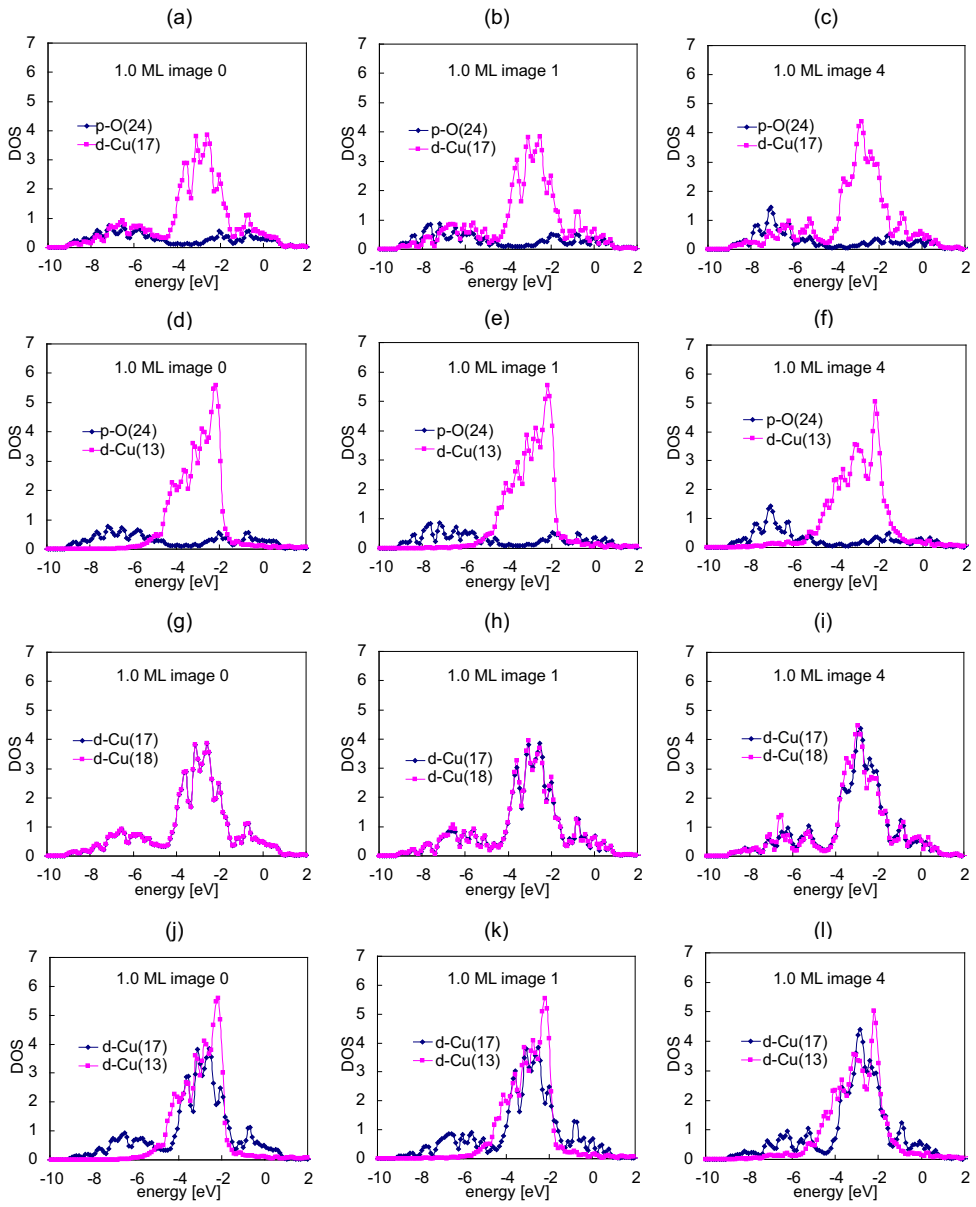

Figure 30: Comparison of DOS about p-orbital of oxygen atom [p-O(index number)] and d-orbital of copper atom [d-Cu(index number)] in the transition structures of $p(2\times2)$ surface structure at the oxygen coverage of 1.0ML (The index of transition structure is shown in each plot and Fig. 27(b).); The vertical position of the embedding oxygen decreases along increasing index number of images from left to right. The first row of plots [from Fig. 30(a) to 30(c)] show the DOS comparison between the embedding oxygen atom and its nearest neighboring copper atom. The second row [from Fig. 30(d) to 30(f)] show the DOS comparison of between the embedding oxygen atom and the copper atom (in the second copper layer from the topmost copper layer) beneath the embedding oxygen atom. The third row [from Fig. 30(g) to 30(i)] shows DOS comparison of d-orbitals of copper atoms in the topmost layer along the oxygen embedment. In same manner, the fourth row [from Fig. 30(j) to 30(l)] shows DOS comparison of d-orbitals of copper atom between the topmost and second copper layer along the oxygen embedment.

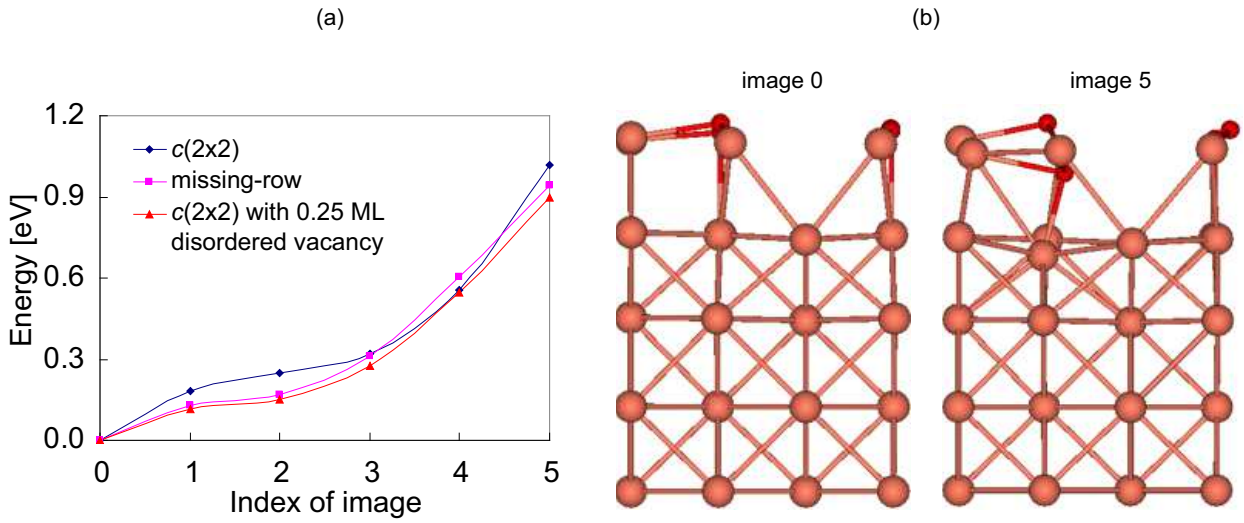

Figure 31: (a) Total system energies in each image predicted by neb calculation for different surface morphologies in $p(2\sqrt{2}\times2\sqrt{2})$ unit cell (The vertical step size is 0.26 Å for the $c(2\times2)$, and 0.19 Å for the missing-row reconstruction and the $c(2\times2)$ with 0.25 ML disordered vacancy structures between adjacent images). (b) Transition structure of image 0 and image 5 from the missing-row reconstruction.

different [see Fig. 30(h)] and the differences increases as the oxygen atom embeds [see Fig. 30(i)]. In comparison of d-orbitals between the topmost and second copper layer, the oxygen embedment makes the maximum DOS of d-orbitals in the topmost layer increase but that of the second copper layer decrease. [see Figs. 30(j), 30(k), and 30(l).]

For the $p(2\sqrt{2}\times2\sqrt{2})$ unit cell at 0.5 ML coverage, the NEB method results are shown in Fig. 31. In this work, the surfaces have the same oxygen coverage of 0.5 ML, but they have different surface morphology: $c(2\times2)$, missing-row reconstruction, and $c(2\times2)$ with 0.25 ML

Surface morphology at 0.5 ML	$c(2\times2)$ unreconstructed surface	missing row reconstruction	$c(2\times2)$ with 0.25 ML disordered vacancy
Energy difference [eV]	1.017	0.941	0.899
Energy barrier [eV]	-	-	-

Table 9: Energy difference and energy barrier calculated by NEB for an oxygen embedment in the $p(2\sqrt{2}\times2\sqrt{2})$ unit cell of Cu(100) surface with different surface morphologies; Energy difference is calculated by subtracting total system energy of image 0 (initial state) from that of image 5 (final state) for all surface morphology. Because there is no local maxima of total system energy, energy barrier is not allowed to be calculated in these cases.

disordered vacancy.

As shown in Fig. 31(a), the oxygen embedment increases the total system energy for all surface morphologies in a similar manner. The energy difference for each case is shown in Table 9. There is no local maxima in Figs. 31(a), 31(c), and 31(e). The biggest energy difference is in the case of $c(2\times2)$ and the smallest energy difference is in the case of $c(2\times2)$ with 0.25 ML disordered vacancy but the difference between the maximum and the minimum energy difference is only 0.118 eV.

Although no energetically favorable state is found by embedding oxygen into the missing-row reconstructed Cu(100) surface, I believe that there must be a transition state from the missing-row reconstruction to copper (II) oxide island formation. In the the unreconstructed Cu(100) surface, as the surface oxygen coverage increases, the energetically favorable sites are found between the top and second copper layer. Likew, an unknown factor might make the energetics of the missing-row reconstructed Cu(100) surface favorable to the oxygen embedment. Therefore, further investigation will be performed for the oxygen embedment into the missing-row reconstructed Cu(100) surface.

5.4 Proposed research

To find the energetically favorable transition states by embedding oxygen into the missing-row reconstructed Cu(100) surface, I will investigate three different initial positions for the oxygen embedment, as shown in Fig. 32. I expect that the positions at missing-row (position 1 and 3) should have less effect from the second copper layer for the oxygen embedment because of the missing-row, and position 2 will attract a diffusive oxygen atom because the unoccupied four-fold hollow site is energetically favorable for the oxygen adsorption.

I will also place a point defect in the topmost copper layer and investigate the energetics by embedding an oxygen atom. If I find a further oxygen-induced reconstruction based on the proposed work provided in Section 4.3, the further reconstructed structure on the missing-row reconstructed Cu(100) surface will be applied for this oxygen embedment investigation. For

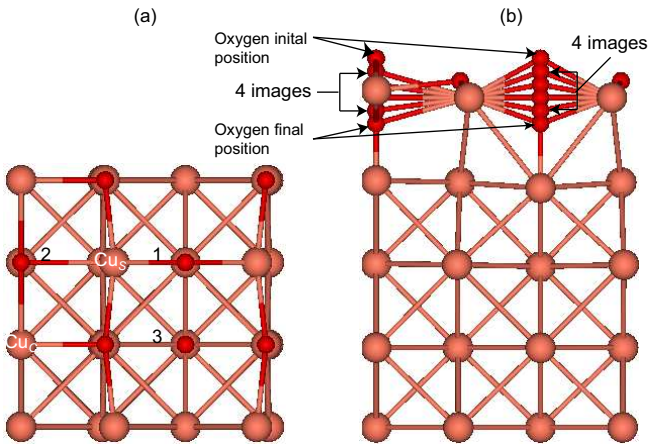

Figure 32: (a) Top and (b) Side view of $p(2\sqrt{2}\times2\sqrt{2})$ unit cell with four images for NEB calculation. Three new embedment initial positions will be investigated by NEB method. 1. Missing-row site between copper atoms at step-edge. 2. Unoccupied four-fold hollow site. 3. Missing-row site between surface-adsorbed oxygen atoms.

example, a copper atom at a step-edge (Cu_S) or a copper atom between surface-adsorbed oxygen atoms (Cu_C) will be removed [see Fig. 32(a)] and the unit cell (with the point defect) will be relaxed for the initial and final state for the oxygen embedment investigation. Then the energetics and transition structures will be investigated by NEB method. For the minimum vertical position of the oxygen embedment, single point calculation will be performed for various oxygen embedding depth. DOS calculation will follow to compare the change between the before and the after oxygen embedment in the point of electronic structure. Then, I will also investigate two oxygen atoms embedment in same time and compare the transition structures and energetics for more complicated case.

6 Molecular dynamics simulation of metal-oxide systems

Predicting the conditions that exist at a metal-oxide interface is challenging due to a transition in the nature of the atomic bonds. To investigate such a system, we implemented a charge transfer interatomic potential into a molecular dynamics (MD) simulation. To start, I performed MD simulation based on the Zhou potential[78,79] for the Al/α-Al_2O_3 interface. For the Cu/Cu_2O interface, a new interatomic potential is being developed by collaborative work with the University of Florida based on the charge-optimized many-body[80] (COMB) framework. The potential currently works for bulk copper and Cu_2O. In the proposed work, I will apply DFT method to help develop and validate the potential for interfacial systems.

6.1 Introduction to MD simulation

Molecular dynamics simulation is a computer technique that applies Newton's laws of motion and interatomic force fields.[81–83] MD simulation can be used to predict the charges around metal-oxide interfaces with interatomic potential functions that include dynamic charge transfer.

Dynamic charge transfer is a theoretical technique to realize the interaction between the cations and anions of a metal oxide system in an MD simulation. The implementation of a charge transfer scheme in a MD simulation is based on the assumption that the electrostatic energy of the system will be minimized at every simulation time step. This assumption is justified under the Born-Oppenheimer approximation, which states that the electronic degrees of freedom are much faster than the atomic or ionic degrees of freedom. To find the equilibrium charge, the electrostatic energy is minimized. Typical methods to find the charge to minimize electrostatic energy are explicit techniques based on matrix inversion, but they require very expensive computation and they are not practical for the large systems. As an alternative, we construct a modified equation of motion based on charge to minimize the

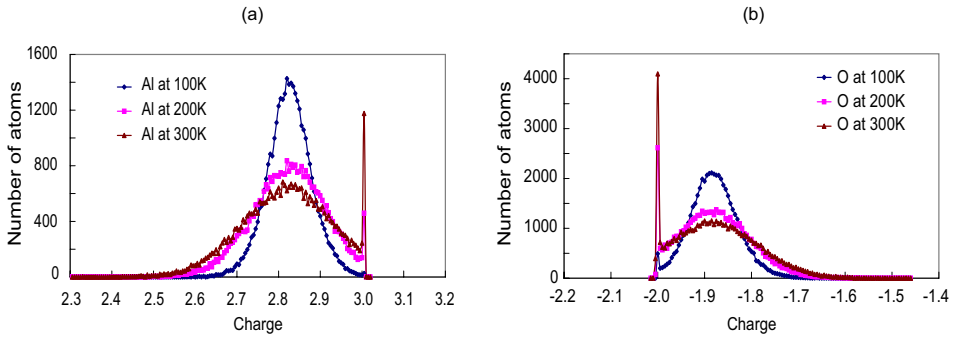

Figure 33: Charge distribution of bulk α-Al_2O_3 predicted by MD simulation based on charge transfer interatomic potential at different temperature; (a) Charge distribution of aluminum. (b) Charge distribution of oxygen

electrostatic energy based on Rick *et al.*[84]

I implemented the Charge Transfer Inter-atomic Potential (CTIP) based on the formulism developed by Zhou *et al.*[78,79] with dynamic charge transfer[84] and predicted the charge distribution in the bulk α-Al_2O_3 and across the Al/α-Al_2O_3 interface. My colleague in the University of Florida performed MD simulations based on the COMB[80] framework for bulk copper, bulk Cu_2O, and oxygen adsorption on the Cu(100) surface. Those preliminary results are shown in the following sections.

6.2 Preliminary results

6.2.1 Interatomic potential for Al/Al_2O_3 interface

I have plotted the charge distribution in bulk α-Al_2O_3 in Fig. 33. Equilibrium charges are predicted for the aluminum and oxygen with a charge barrier. The charge barrier is based on the concept that the charge on an atom must be bounded by its valence.[79] In our MD simulation, the bounded charge concept is realized by the charge barrier. As shown in Fig. 33, the aluminum and oxygen charge distributions are similar to normal distributions but the charges are bound within the min - max range for each species.

Aluminum is a fcc crystal with a lattice constant of 4.05Å.[85] α-Al_2O_3 is hexagonal closed pack (hcp) with lattice planar constants a=4.74Å.[86] The different structure and lattice prop-

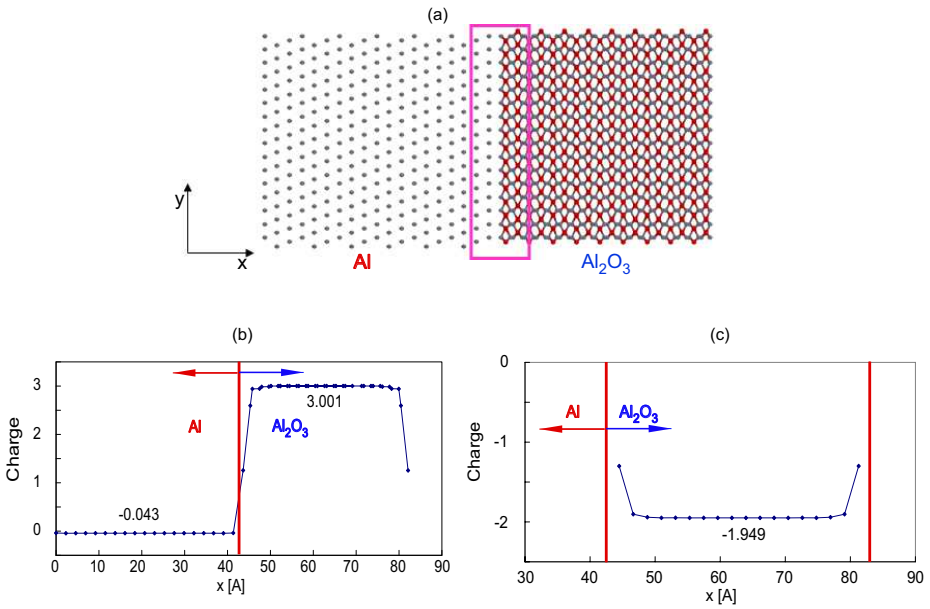

Figure 34: Charge distribution of Al/α-Al_2O_3 interface predicted by MD simulation based on charge transfer interatomic potential; (a) Al/α-Al_2O_3 interface structure (To compensate the lattice mismatch between Al slab and α-Al_2O_3 slab, the region of Al slab inside the rectangle is strained). (b) Charge distribution of aluminum. (c) Charge distribution of oxygen

erties make a mismatch between aluminum and α-Al_2O_3 , as shown in the rectangle of Fig. 34(a). In my MD simulation, I strained a metal aluminum slab and attached it to a slab of α-Al_2O_3 to compensate for the mismatch at the Al/α-Al_2O_3 interface.

The predicted charge distributions of aluminum and oxygen around the Al - Al_2O_3 interface are shown in Figs. 34(b) and 34(c). The aluminum charge increases gradually through interface and converges to +3 in α-Al_2O_3 slab as shown Fig. 34(b). The oxygen charge decreases as the distance from the interface increases, and converges to -2 in the α-Al_2O_3 slab. The charge value for aluminum makes sense because it should be around zero in aluminum for neutral state in pure metal and +3 in alumina for ionic bonding between Al and O ions.

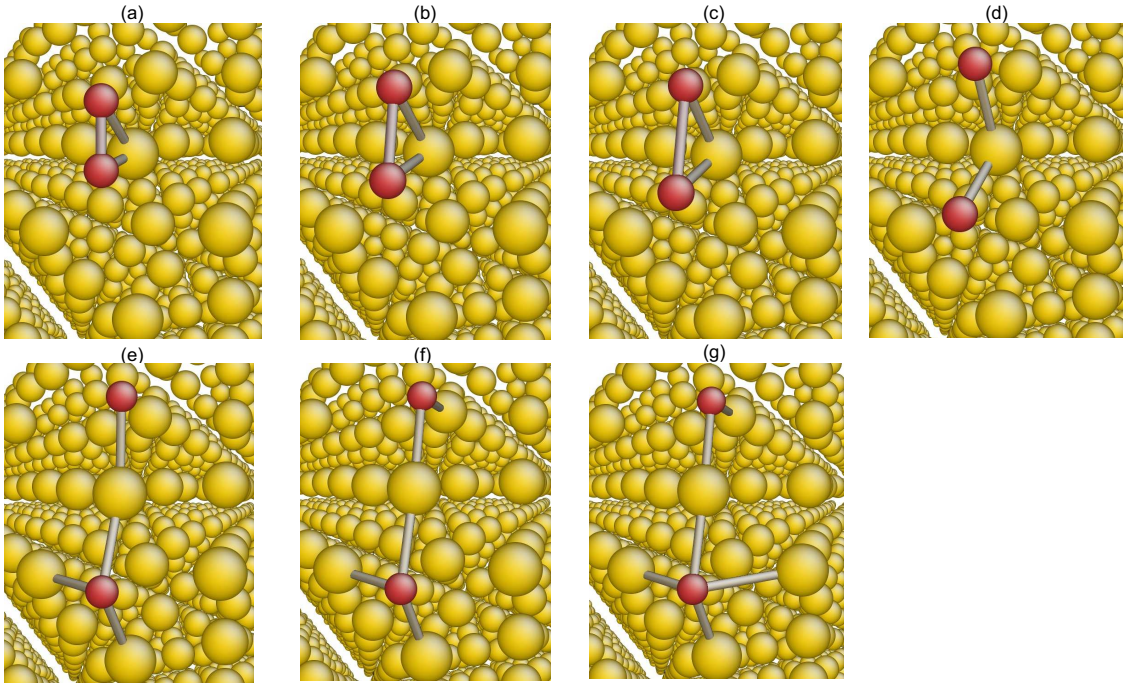

Figure 35: Oxygen molecule dissociation and atomic oxygen adsorption on the Cu(100) surface predicted by molecular dynamic simulation based on COMB framework (The time interval is 11.04 fs between each figure. Two small spears (red) are oxygen and others (yellow) are copper atoms.); (a) Molecular oxygen adsorption on top site. (b)-(d) Dissociation. (e)-(g) Atomic oxygen adsorption on four-fold hollow site.

6.2.2 Interatomic potential for Cu/Cu_2O interface

The molecular dynamics (MD) simulations of Cu/Cu_2O interface systems are performed by my colleague at the University of Florida based on the COMB[80] framework. Snapshots of a dissociation/adsorption process from an MD simulation are shown in Fig. 35. Figs. 35(a), 35(b), 35(c), and 35(d) show that the top site attracts and dissociates an oxygen molecule. Two oxygen atoms from the dissociated oxygen molecule are attracted by copper atoms [see Figs. 35(e) and 35(f)] and eventually adsorbed at four-fold hollow sites, as shown in Figs. 35(g). This result corresponds well with my hypothesis based on the adsorption energy calculation shown in Section 3.2.

The bulk properties of copper and Cu_2O predicted by the COMB[80] framework and compared to both experimental result and DFT calculation, as shown in Table 10. The bulk properties predicted by the MD simulation show very good agreement with the experimen-

Property	Copper			Cu_2O		
	Exp	DFT	MD	Exp	DFT	MD
a_0 [Å]	3.60[38,66]	3.65	3.61	4.27[87]	4.31	4.27
E_c [eV/atom]	-3.49[88]	-3.50	-3.53	-1.75[65]	-	-2.04
B [GPa]	137[88]	140	139	112[89]	113	115
C_{11} [GPa]	176[90]	173	172	126[89]	126	129
C_{12} [GPa]	125[90]	123	122.6	109[89]	106	108
C_{44} [GPa]	82[90]	80	50	14[89]	15	19

Table 10: . Bulk properties of copper and Cu_2O predicted by experiment, DFT, and MD simulation. [a_0 = lattice constant, E_c = cohesive energy, B = bulk modulus, and elastic constants (C_{11}, C_{12}, and C_{44})]

tal results and DFT calculation in general. The fitting for the Cu/Cu_2O interface is not performed yet and is a part of my proposed work.

6.3 Proposed research

Molecular dynamics simulations requires much less computation than DFT calculation and can handle much bigger structures and larger simulations. In addition, temperature, which can not be considered in a typical DFT method, is naturally included in MD simulation. It is for theses reasons that we want to develop an interatomic potential for the Cu/Cu_2O interface.

To develop the Cu/Cu_2O interatomic potential, I will make feed back loop based on DFT method. My colleague in UF will perform MD simulation and we will compare MD simulation results to my DFT results such as adsorption energy and the energy barrier for an oxygen embedment on the different surfaces at different oxygen coverage and change those parameters until we have reasonable agreement between MD simulation and DFT results.

7 Outcomes and schedule

The outcomes of my proposed research will be:

1. Identification of the early transition states between reconstruction and oxide growth on the Cu(100) and Cu(110) surfaces,

2. The energy barrier for oxygen embedment into different adsorption sites with different oxygen coverage and surface morphology on the missing-row reconstructed Cu(100) surface,

3. A validation of a Cu/Cu_2O interatomic potential by predictions from DFT calculation.

4. Input parameters for the KMC code

The schedule for this proposed research is shown in Fig. 36.

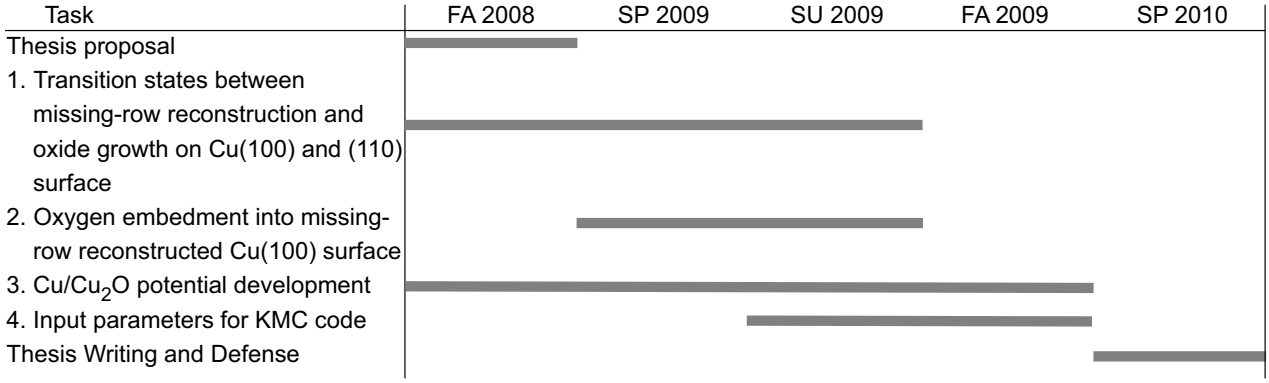

Figure 36: The expected schedule for the proposed research

8 Biographical sketch

Minyoung Lee was born and grew up in Suwon, South Korea. He obtained a Bachelor of Science degree in mechanical engineering from Seoul National University in Feb. 2001. He worked as a quality engineer for Korean Air Aerospace division from Jan. 2001 to June. 2004. He entered Carnegie Mellon in Fall 2004 and received a Masters of Science degree in Spring 2006.

Coursework at Carnegie Mellon

Mathematical Techniques in Mechanical Engineering, Fall 2004

Advanced Heat Transfer, Fall 2004

Convective Heat Transfer, Spring 2005

Small Scale Heat Transfer, Spring 2005

Engineering Vibrations, Spring 2005

Introduction to Solid Mechanics I, Fall 2005

Molecular Simulation of Materials, Spring 2006

Advanced Fluid Mechanics I, Fall 2006

Advanced Thermodynamics I, Fall 2006

Statistical Thermodynamics, Spring 2007

Applied Electronic Structure Theory, Fall 2007 (at the University of Pittsburgh)

Introduction to Parallel Computing and Scientific Computation, Spring 2008

Materials for Energy Storage, Spring 2008

Conference Presentations

1. M. Y. Lee, A. J. H. McGaughey, S. Sinnott, S. Phillpot, and J. C. Yang, "Modeling the early stage of copper oxidation by *ab initio* calculation," to be presented at 2008 MRS Fall Meeting, December 2008, Boston, MA.

2. M. Y. Lee, W. Liu, and M. Asheghi, "A Novel Scheme in Thermal Modeling of Printed Circuit Boards," presented at InterPACK 2005 Conference, July 2005, San Francisco, CA.

References

[1] L. Cecchi, F. D. Sarlo, and F. Machetti, "Synthesis of 4,5-dihydroisoxazoles by condensation of primary nitro compounds with alkenes by using a copper/base catalytic system." *Chemistry - A European Journal* **14** (2008) 7903–7912.

[2] W. Setthapun, S. K. Bej, and L. T. Thompson, "Carbide and nitride supported methanol steam reforming catalysts: Parallel synthesis and high throughput screening." *Topic in Catalysis* **49** (2008) 73–80.

[3] L. Zhen, W. Guan, L. Shang, M. Liu1, and G. Liu, "Organic thin-film transistor memory with gold nanocrystals embedded in polyimide gate dielectric." *Journal of Physics D: Applied Physics* **41** (2008) 135111–1–5.

[4] N. Cabrera and N. F. Mott, "Theory of the oxidation of metals." *Reports on Progress in Physics* **12** (1948) 163–184.

[5] J. C. Yang, B. Kolasa, J. M. Gibson, and M. Yeadon, "Self-limiting oxidation of copper." *Applied Physics Letters* **73** (1998) 2841–2843.

[6] G. Zhou and J. C. Yang, "Initial oxidation kinetics of cu(100), (110), and (111) thin films investigated by in situ ultra-high-vacuum transmission electron microscopy." *Journal of Materials Research* **20** (2005) 1684–1694.

[7] G. Zhou and J. C. Yang, "In situ uhv-tem investigation of the kinetics of initial stages of oxidation on the roughened cu(110) surface." *Surface Science* **559** (2004) 100–110.

[8] G. Zhou and J. C. Yang, "Formation of quasi-one-dimensional cu_2o structures by in situ oxidation of cu(100)." *Physical Review Letters* **89** (2002) 106101–1–4.

[9] G. Zhou and J. C. Yang, "Temperature effect on the cu_2o oxide morphology created by oxidation of cu(0 0 1) as investigated by in situ uhv tem." *Applied Surface Science* **210** (2003) 165–170.

[10] G. M. Whitesides and M. Boncheva, "Beyond molecules: Self-assembly of mesoscopic and macroscopic components." *Proceedings of the National Academy of Sciences of the United States of America* **99** (2002) 4769–4774.

[11] H. C. Zeng, R. A. McFarlane, and K. A. R. Mitchell, "A leed crystallographic investigation of some missing row models for the cu(100)-$(2\sqrt{2} \times \sqrt{2})$r45°-o surface structure." *Surface Science* **208** (1989) L7–L14.

[12] F. Jensen, F. Besenbacher, E. Laegsgaard, and I. Stensgaard, "Dynamics of oxygen-induced reconstruction of cu(100) studied by scanning tunneling microscopy." *Physical Review B* **42** (1990) 9206–9212.

[13] T. Lederer, D. Arvanitis, G. Comelli, L. Troger, and K. Baberschke, "Adsorption of oxyen on cu(100). i. local structre and dynamics for two atomic chemisorption states." *Physical Review B* **48** (1993) 15390–15404.

[14] F. M. Leibsle, "Stm studies of oxygen-induced structures and nitrogen coadsorption on the cu(100) surface: evidence for a one-dimensional oxygen reconstruction and reconstructive interactions." *Surface Science* **337** (1995) 51–66.

[15] T. Wiell, J. E. Klepeis, P. Bennich, O. Bjorneholm, N. Wassdahl, and A. Nilsson, "Local aspects of the adsorbate-substrate chemical bond in n/cu(100) and o/cu(100)." *Physical Review B* **58** (1998) 1655–1664.

[16] D. Sekiba, T. Inokuchi, Y. Wakimoto, K. Yagi-Watanabe, and H. Fukutani, "Electronic structure of cu(100)$(2\sqrt{2}\times\sqrt{2})r$45-o surface: angle-resolved photoemission spectroscopy and tight-binding calculation." *Surface Science* **470** (2000) 43–52.

[17] N. Hartmann and R. J. Madix, "Growth and ordering of cu-o islands during oxygen adsorption on cu(110) at 470 k." *Surface Science* **488** (2001) 107–122.

[18] M. Kittel, M. Polcik, R. Terborg, J.-T. Hoeft, P. Baumgartel, A. Bradshaw, R. Toomes, J.-H. Kang, D. Woodru, M. Pascal, C. Lamont, and E. Rotenberg, "The structure of oxygen on cu(100) at low and high coverages." *Surface Science* **470** (2001) 311–324.

[19] Y. P. Guo, K. C. Tan, H. Q. Wang, C. H. A. Huan, and A. T. S. Wee, "Low-energy electron diffraction study of oxygen-induced reconstructions on cu(210)." *Physical Review B* **66** (2002) 165410–1–8.

[20] Y. Uehara, T. Matsumoto, and S. Ushioda, "Identification of o atoms on a cu(110) surface by scanning tunneling microscope light emission spectra." *Physical Review B* **66** (2002) 075413–1–5.

[21] D. Loffreda, A. D. Corso, S. Baroni, L. Savio, and M. R. Luca Vattuone b, "Oxygen vibrations in o/ag(001)." *Surface Science* **530** (2003) 26–36.

[22] M. Hirsimaki, M. Lampima, K. Lahtonen, I. Chorkendorff, and M. Valden, "Investigation of the role of oxygen induced segregation of cu during cu_2o formation on cu100, ag/cu100 and cu(ag) alloy." *Surface Science* **583** (2005) 157–165.

[23] L. Sun and J. Yang, "The low-temperature initial oxidation stages of cu(100) investigated by in situ ultra-high-vacuum transmission electron microscopy." *Journal of Materials Research* **20** (2005) 1910–1917.

[24] M. J. Harrison, D. P. Woodruff, J. Robinson, W. P. D. Sander, and J. Kirschner, "Adsorbate-induced surface reconstruction and surface-stress changes in cu(100)/o: Experiment and theory." *Physical Review B* **74** (2006) 165402–1–7.

[25] K. Moritani, M. Okada, T. Fukuyama, Y. Teraoka, A. Yoshigoe1, and T. Kasai, "The azimuthal dependent oxidation process on cu(110) by energetic oxygen molecules." *The European Physical Journal D* **38** (2006) 111–115.

[26] H. Iddir, D. D. Fong, P. Zapol, P. H. Fuoss, L. A. Curtiss, G.-W. Zhou, , and J. A. Eastman, "Order-disorder phase transition of the cu(001) surface under equilibrium oxygen pressure." *Physical Review B* **76** (2007) 241404(R)–1–4.

[27] P. S. Bagus and F. Illas, "Theoretical analysis of the bonding of oxygen to cu(100)." *Physical Review B* **42** (1990) 10852–10857.

[28] K. W. Jacobsen and J. K. Norskov, "Theory of the oxygen-induced restructuring of cu(110) and cu(100) surfaces." *Physical Review Letter* **65** (1990) 1788–1791.

[29] H. Agren, V. VCarravetta, and L. G. M. Pettersson, "Static exchange and cluster modeling of core electron shakeup spectra of surface adsorbates: Co/cu(100)." *Physical Review B* **53** (1996) 16074–16085.

[30] F. Frechard and R. van Santen, "Theoretical study of the adsorption of the atomic oxygen on the cu(110) surface." *Surface Science* **407** (1998) 200–211.

[31] J. Gomes and J. Gomes, "Adsorption of the formate species on copper surfaces: a dft study." *Surface Science* **432** (2003) 279–290.

[32] S. Liem, J. Clarke, and G. Kresse, "Pathways to dissociation of o_2 on cu (110) surface: first principles simulations." *Surface Science* **459** (2000) 104–114.

[33] Y. Xu and M. Mavrikakis, "Adsorption and dissociation of o_2 on cu(111): thermochemistry, reaction barrier and the effect of strain." *Surface Science* **494** (2001) 131–144.

[34] S. Stolbov, A. Kara, and T. S. Rahman, "Electronic structure of the c(2x2)o/cu(001) system." *Physical Review B* **66** (2002) 245405–1–8.

[35] S. Stolbov and T. S. Rahman, "Role of long range interaction in oxygen superstructure formation on cu(001) and ni(001)." *Physical Review Letters* **89** (2002) 116101–1–4.

[36] L. Padilla-Campos and P. Fuentealba, "Theoretical study of the adsorption of oxygen on a cu(100) surface and the coadsorption with alkali atoms." *Theoretical Chemistry Accounts* **110** (2003) 414–420.

[37] Z. X. Wang and F. H. Tian, "The adsorption of o atom on cu (100), (110), and (111) low-index and step defect surfaces." *Journal of Physical Chemistry B* **107** (2003) 6153–6161.

[38] M. Alatalo, S. Jaatinen, P. Salo, and K. Laasonen, "Oxygen adsorption on cu(100): First-principles pseudopotential calculations." *Physical Review B* **70** (2004) 245417–1–6.

[39] A. Puisto, *Oxygen adsorption on clean and oxygen precovered Cu(100)*. Ms thesis, Lappeenranta University of Technology, Lappeenranta, Finland (2004), see also http://www.ee.lut.fi/fi/lab/elemat/julkaisut/masters thesis apuisto.pdf.

[40] C. D. Valentin, A. Figini, and G. Pacchioni, "Adsorption of no and no_2 on terrace and step sites and on oxygen vacancies of the cao(100) surface." *Surface Science* **556** (2004) 145–158.

[41] L. Jiang, G.-C. Wang, Z.-S. Cai, Y.-M. Pan, and X.-Z. Zhao, "Promotion of the water-gas shift reaction by pre-adsorbed oxygen on cu(hkl) surfaces: a theoretical study." *Journal of Molecular Structure (Theochem)* **710** (2004) 97–104.

[42] T. Kangas, K. Laasonen, A. Puisto, H. Pitkanen, and M. Alatalo, "On-surface and sub-surface oxygen on ideal and reconstructed cu(100)." *Surface Science* **584** (2005) 62–69.

[43] A. Puisto, H. Pitkanen, M. Alatalo, S. Jaatinen, P. Salo, A. S. Foster, T. Kangas, and K. Laasonen, "Adsorption of atomic and molecular oxygen on cu(100)." *Catalysis Today* **100** (2005) 403–406.

[44] M. Alatalo, A. Puisto, H. Pitkanen, A. Foster, and K. Laasonen, "Adsorption dynamics of o_2 on cu(100)." *Surface Science* **600** (2006) 1574–1578.

[45] N. Bonini, A. Kokalj, A. D. Corso, S. de Gironcoli, and S. Baroni, "Structure and dynamics of the missing-row reconstruction on o/cu(001) and o/ag(001)." *Surface Science* **600** (2006) 5074–5079.

[46] S. J. J. Blomqvist, P. Salo, A. Puisto, M. Alatalo, M. Hirsimaki, M. Ahonen, and M. Valden, "Adsorption and diffusion dynamics of atomic and molecular oxygen on reconstructed cu(100)." *Physical Review B* **74** (2007) 075402–1–8.

[47] N. Nivalainen, *Oxygen adsorption on Cu(211) and structurally and chemically modified Cu(100)*. Ms thesis, Lappeenranta University of Technology, Lappeenranta, Finland (2007), see also http://www.ee.lut.fi/fi/lab/elemat/julkaisut/masters thesis nivalainen.pdf.

[48] A. Puisto, *The Initial Oxidation of Transition Metal Surfaces*. Phd thesis, Lappeenranta University of Technology, Lappeenranta, Finland (2008).

[49] T. Fujita, Y. Okawa, Y. Matsumoto, and K. ichi Tanaka, "Phase boundaries of nanometer scale c(2x2)-o domains on the cu(100) surface." *Physical Review B* **54** (1996) 2167–2174.

[50] C. Q. Sun, "Oxidation electronics: bond-band-barrier correlation and its applications." *Progress in Materials Science* **48** (2003) 521–685.

[51] P. Hohenberg and W. KOHN, "Inhomogeneous electron gas." *Physical Review* **136** (1964) B864–B871.

[52] W. Kohn and L. J. Sham, "Self-consistent equation including exchange and correlation effects." *Physical Review* **140** (1965) A1133–A1138.

[53] G. Kresse and J. Hafner, "Norm-conserving and ultrasoft pseudopotentials for fisrt-row and tranition elements." *Journal of Physics: Condensed Matter* **6** (1994) 8245–8257.

[54] D. Young, *Computational Chemistry: A Practical Guide for Applying Techniques to Real World Problems Appendix A. A.2.1 pg 332, ADF*. Wiley-Interscience, New York (2001).

[55] X. Gonze, J.-M. Beuken, R. Caracas, F. Detraux, M. Fuchs, G.-M. Rignanese, L. Sindic, M. Verstraete, G. Zerah, F. Jollet, M. Torrent, A. Roy, M. Mikami, P. Ghosez, J.-Y. Raty, and D. Allan, "First-principles computation of material properties: the abinit software project." *Computational Materials Science* **25** (2002) 478–492.

[56] J. M. Soler, E. Artacho, J. D. Gale, A. Garcia, J. Junquera, P. Ordejon, and D. Sanchez-Portal, "The siesta method for ab initio order-n materials simulation." *Journal of Physics: Condensed Matter* **14** (2002) 2745–2779.

[57] M. F. Guest, I. J. Bush, H. J. J. van Dam, P. Sherwood, J. M. H. Thomas, J. H. van Lenthe, R. W. A. Havenith, and J. Kendrick, "The gamess-uk structure package: algorithms, developments and applications." *Molecular Physics* **103** (2005) 719–747.

[58] G. Kresse and J. Furthmuller, "Efficiency of ab-initio total energy calculations for metals and semiconductors using a plane-wave basis set." *Computational Materials Science* **6** (1996) 15–50.

[59] G. Kresse and J. Furthmuller, "Efficient iterative schemes for ab-initio total-energy calculations using a plane-wave basis set." *Physical Review B* **54** (1996) 11169–11186.

[60] J. P. Perdew, J. A. Chevary, S. H. Vosko, K. A. Jackson, M. R. Pederson, D. J. Singh, and C. Fiolhais, "Atoms, molecules, solids, and surfaces: Applications of the generalized gradient approximation for exchange and correlation." *Physical Review B* **46** (1992) 6671–6687.

[61] J. P. Perdew, K. Burke, and M. Ernzerhof, "Generalized gradient approximation made simple." *Physical Review Letters* **77** (1996) 3865–3868.

[62] H. J. Monkhorst and J. D. Pack, "Special points for brillouin-zone integrations." *Physical Review B* **13** (1976) 5188–5192.

[63] F. R. Kroeger and C. A. Swenson, "Absolute linear thermal-expansion measurements on copper and aluminum from 5 to 320k." *Journal of Applied Physics* **48** (1977) 853–864.

[64] A. K. Giri and G. B. Mitra, "Extrapolated values of lattice constantso f some cubic metals at absolute zero." *Journal of Physics D: Applied Physics* **18** (1985) L75–L782.

[65] D. R. Lide, *CRC Handbook of Chemistry and Physics, Student Edition. 84th Edition.* CRC Press, New York (2004).

[66] J. Greeley, A. Gokhale, J. Kreuser, J. Dumesic, H. Topsoe, N.-Y. Topsoe, and M. Mavrikakis, "Co vibrational frequencies on methanol synthesis catalysts: a dft study." *Journal of Catalysis* **213** (2003) 63–72.

[67] T. L. Cottrell, *The Strengths of Chemical Bonds, 2nd ed.* Butterworths, London (1958).

[68] B. D. Darwent, *National Standard Reference Data Series.* National Bureau of Standards, No. 31, Washington, DC (1970).

[69] L. Pauling, "The nature of the chemical bond. iv. the energy of single bonds and the relative electronegativity of atoms." *Journal of American Chemical Society* **54** (1932) 3570–3582.

[70] F. Jensen, F. Besenbacher, E. Laegsgaard, and I. Stensgaard, "Surface reconstruction of cu(110) induced by oxygen chemisorption." *Physical Review B* **41** (1990) 10233–10236.

[71] Y. Kuk, F. M. Chua, P. J. Silverman, and J. A. Meyer, "O chemisorption on cu(11) by scanning tunneling microscopy." *Physical Review B* **41** (1990) 12393–12402.

[72] A. Soon, M. Todorova, B. Delley, and C. Stampfl, "Oxygen adsorption and stability of surface oxides on cu(110): A first-principles investigation." *Physical Review B* **73** (2006) 165424–1–12.

[73] X.-Y. Pang, L.-Q. Xue, and G.-C. Wang, "Adsorption of atoms on cu surfaces: a density functional theory study." *Langmuir* **23** (2007) 4910–4917.

[74] H. Jonsson, G. Mills, and K. W. Jacobsen, *Classical and Quantum Dynamics in Condensed Phase Simulations edited by B. J. Berne, G. Ciccotti, and D. F. Coker.* World Scientific, Singapore (1998).

[75] G. Henkelman and H. Jonsson, "Improved tangent estimate in the nudged elastic band method for finding minimum energy paths and saddle points." *Journal of Chemical Physics* **113** (2000) 9978–9985.

[76] T. Fordell, P. Salo, , and M. Alatalo, "Self-diffusion on fcc (100) metal surfaces: Comparison of different approximations." *Physical Review B* **65** (2002) 233408–1–4.

[77] Vienna Ab-initio Simulation Package (VASP) the guide, March 2007, Available online at http://cms.mpi.univie.ac.at/vasp/vasp/vasp.html.

[78] X. W. Zhou, H. N. G. Wadley, J. S. Folhol, and M. N. Neurock, "Modified charge transfer.embedded atom method potential for metalometal oxide systems." *Physical Review B* **69** (2004) 035402–1–20.

[79] X. W. Zhou and H. N. G. Wadley, "A charge transfer ionic.embedded atom method potential for the o-al-ni-co-fe system." *Journal of Physics: Condensed Matter* **17** (2005) 3619–3635.

[80] J. Yu, S. B. Sinnott, and S. R. Phillpot, "Charge optimized many-body potential for the si/sio_2 system." *Physical Review B* **75** (2007) 085311–1–13.

[81] M. P. Allen and D. J. Tildesley, *Computer Simulation of Liquids*. Clarendon Press: Oxford. UK (1987).

[82] H. C. Andersen, "Molecular dynamics simulations at constant pressure and/or temperature." *Journal of Chemical Physics* **72** (1980) 2384–2393.

[83] Y. Mishin, D. Farkas, M. J. Mehl, and D. A. Papaconstantopoulos, "Interatomic potentials for monoatomic metals from experimental data and ab initio calculations." *Physical Review B* **59** (1999) 3393–3407.

[84] S. W. Rick, S. J. Stuart, and B. J. Beme, "Dynamical fluctuating charge force fields: Application to liquid water." *Journal of Chemical Physics* **101** (1994) 6141–6156.

[85] W. Witt. *Zeitschrift fur Naturforschung A* **22A** (1967) 92.

[86] P. Dorsey, S. A. Oliver, and C. Vittoria, "Novel technique for ferrimagnetic resonance measurements." *IEEE Transactions On Magnetics* **28** (1992) 2450–2452.

[87] P. Markworth, X. Liu, J. Dai, W. Fan, T. Marks, and R. Chang, "Coherent island formation of cu_2o films grown by chemical vapor deposition on mgo(110)." *Journal of Materials Research* **16** (2001) 2408–2414.

[88] C. Kittel, *Introduction to solid state physics, 7th ed.* John Wiley and sons, Inc., New York (1996).

[89] M. M. Beg and S. M. Shapiro, "Study of phonon dispersion relations in cuprous oxide by inelastic neutron scattering." *Physical Review B* **13** (1976) 1728–1734.

[90] S. G. O'Hara and B. J. Marshall, "Elastic constants of copper-rich alloys with gold." *Physical Review B* **3** (1971) 4002–4006.